



# RESEARCH MEMORANDUM

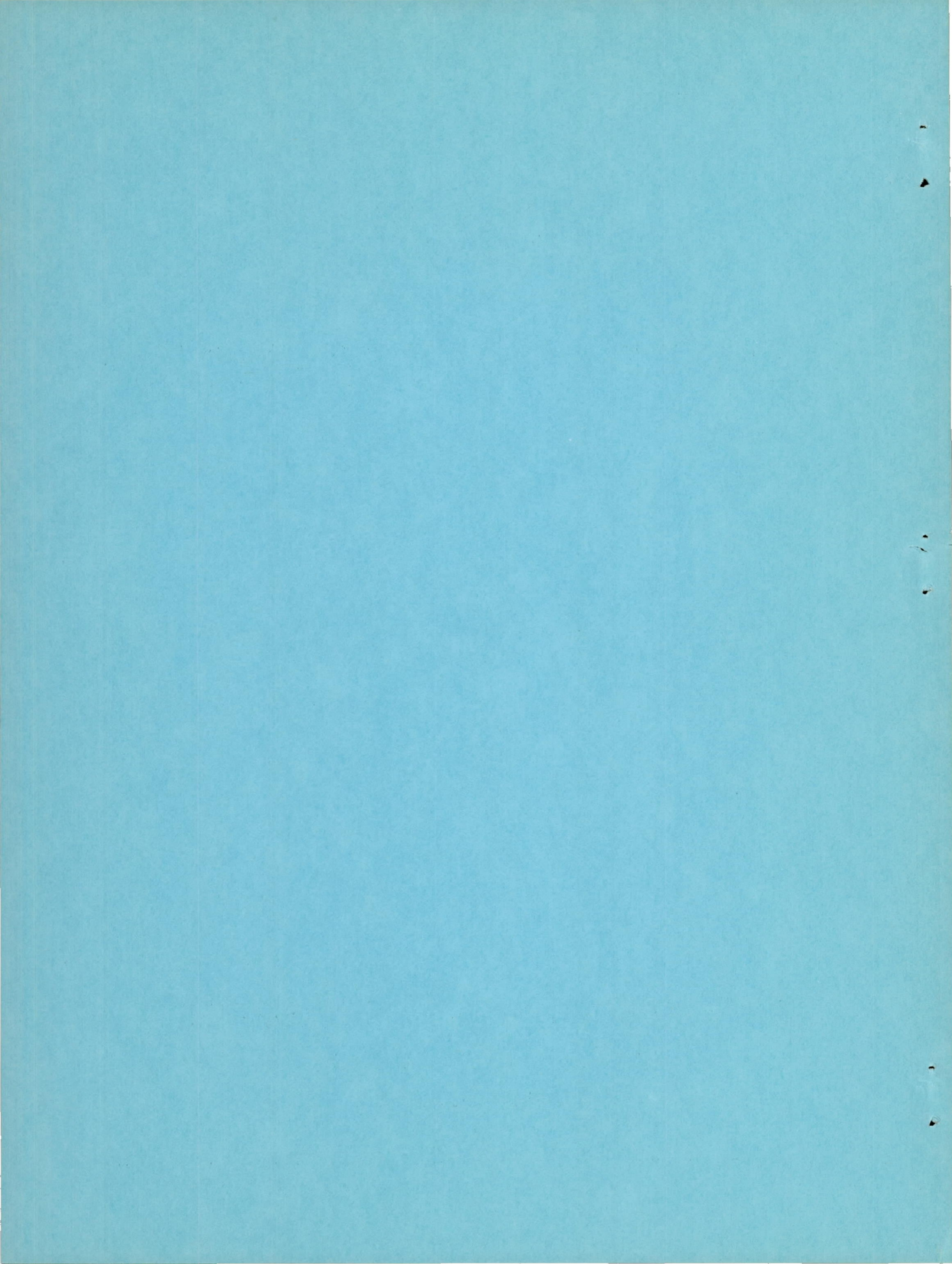
AN INVESTIGATION OF SUBMERGED AIR INLETS ON A 1/4-SCALE  
MODEL OF A TYPICAL FIGHTER-TYPE AIRPLANE

By Noel K. Delany

Ames Aeronautical Laboratory  
Moffett Field, Calif.

NATIONAL ADVISORY COMMITTEE  
FOR AERONAUTICS

WASHINGTON  
June 2, 1948



NATIONAL ADVISORY COMMITTEE FOR AERONAUTICS

RESEARCH MEMORANDUM

AN INVESTIGATION OF SUBMERGED AIR INLETS ON A 1/4-SCALE  
MODEL OF A TYPICAL FIGHTER-TYPE AIRPLANE

By Noel K. Delany

SUMMARY

Wind-tunnel tests were made of submerged air inlets on the fuselage of a 1/4-scale model of a typical fighter-type airplane. The results are presented for ramp plan forms with parallel and with diverging walls and show the effect of the duct-entrance location (forward of the wing and over the wing), internal ducting efficiency, and deflectors.

The air inlets having the ramps with diverging walls were satisfactory in both locations tested on the fuselage, providing high ram pressure recoveries at the simulated entrance to the compressor, high predicted critical Mach numbers, and low external drags. The submerged air inlets with parallel ramp walls had lower ram pressure recoveries for the normal operating range. The ram pressure recovery ratios measured at the inlets were higher for the forward location of the inlets than for the aft location. For an assumed engine position, however, the aft location of the inlets with the shorter, more efficient internal ducts gave the higher ram recoveries at the simulated compressor for the test conditions.

INTRODUCTION

The early development of NACA submerged air inlets was conducted with the submerged inlets installed in the flat wall of a wind tunnel (references 1 and 2). The results of these tests indicated that it should be feasible to design an efficient air-induction system with twin submerged inlets installed on the sides of the fuselage. Placing the submerged inlets on the sides of the fuselage ahead of the jet engine results in a short, straight internal ducting system (references 3 and 4). As the submerged inlets will not protrude outside of the basic fuselage contour they should tend

to eliminate, by inertia separation, foreign material (shell cases, rocks, hail, etc.) from the air inducted into the motor.

The results of reference 3 indicate that the relative location of the wing and the submerged inlets might be critical for inlet performance. The purpose of the tests presented in this report was to investigate the effect of the location of the duct inlets on their characteristics. Two locations were tested, one forward of the wing where the fuselage boundary layer was thin, and the other farther aft on the fuselage and over the point of maximum thickness of the wing. The model was constructed so that, in later tests, the effect of a tractor propeller on the ram recovery could be determined.

The test results presented in this report were obtained in the Ames 7- by 10-foot wind tunnel No. 2 at the request of the Bureau of Aeronautics, Navy Department.

#### SYMBOLS

The symbols used throughout this report are as follows:

A	area, square feet
B	depth of the ramp at the lip, inches
D	drag, pounds
H	total pressure, pounds per square foot
M	Mach number
p	static pressure, pounds per square foot
q	dynamic pressure, pounds per square foot
R	radius of duct, feet
r	radius to a point, feet
S	wing area, square feet
V	stream velocity, feet per second
v	local velocity, feet per second

y	distance perpendicular to a surface, inches
$\delta$	boundary-layer thickness, inches
$\alpha$	model angle of attack with respect to the fuselage reference line, degrees
$\rho$	mass density of the air, slugs per cubic foot

The following subscripts have been used in conjunction with the above symbols:

o	free-stream
1	duct entrance (1.5 in. behind lip leading edge)
2	inlet to the compressor
3	jet exhaust
cr	critical
av	average

The following ratios and coefficients have been used:

$\frac{H-p_o}{H_o-p_o}$	ram recovery ratio
$\frac{V_1}{V_o}$	inlet velocity ratio
$C_{D_{\text{internal}}}$	internal drag coefficient $\left( \frac{\text{internal drag}}{qS} \right)$
$C_{DD}$	external drag coefficient of inlet based on wing area $\left( \frac{\Delta D}{qS} \right)$
$C'_{DD}$	external drag coefficient of inlet based on inlet area $\left( \frac{\Delta D}{qA_1} \right)$

h the height of an area of unit width in which the complete loss of free-stream ram pressure is equivalent to the integrated loss of the total pressure in unit width of the boundary layer

$$\left[ \int_0^{\delta} \left( \frac{H_0 - H}{H_0 - P_0} \right) dy \right]$$

P pressure coefficient  $\left( \frac{P - P_0}{q_0} \right)$

$\eta_D$  internal ducting efficiency  $\left[ 1 - \left( \frac{H_1 - H_2}{H_1 - P_1} \right) \right]$

#### DESCRIPTION OF MODEL

This investigation of twin NACA submerged air inlets was conducted with a 1/4-scale model of a typical high-speed, turbo-propeller driven, fighter-type airplane. In this series of tests the propeller was not used. The pertinent model dimensions and a three-view drawing of the airplane are presented in Appendix A and figure 1, respectively. A photograph of the model mounted in the wind tunnel is shown in figure 2.

The submerged air inlets investigated were designed from the results of reference 2 which indicated that an entrance aspect ratio of 4 and a ramp having an angle of  $7^\circ$  with respect to the fuselage surface and curved diverging walls should produce optimum characteristics. The ramps were submerged in the fuselage so that the ordinates of the ramp below the basic fuselage contour (fig. 3) were equal to those for a  $7^\circ$  ramp below a plane surface. The ramp plan forms tested are given in figure 3 and correspond to those of reference 2. The lips of the duct inlets tested (fig. 4) were the same as the untilted lip of reference 2 but with the mean camber line tilted in  $3^\circ$ . Flush static-pressure orifices were installed on the center line of the ramps and lips of the air intakes.

Two inlet positions, on the sides of the fuselage, were tested. For both positions the horizontal center plane of the inlets was in the horizontal fuselage reference plane (figs. 1 and 3) which was 7.1 percent of the root chord of the wing above the wing upper surface at the point of maximum thickness of the wing at the root. For the forward position of the inlets, the leading edge of the lip was 19.3 percent of the root chord of the wing ahead of the wing leading edge, and for the aft position of the inlets the leading edges of the lips were above the point of maximum thickness of the

wing-root section (35.6 percent chord).

One location of the jet motor was assumed for the airplane. This location allowed a short internal ducting system for the aft location of the inlets and a longer internal ducting system for the forward location. These two internal ducts are shown assembled for preliminary bench tests in figure 5. The long internal duct consisted of the short internal duct with a 14.25-inch, constant-area section added to extend it forward. To provide a more complete comparison of the duct entrances, the forward inlets were also tested with the short internal ducting system. The area ratio between the simulated face of the turbo-jet compressor and the submerged inlets was 1.336 for both the short and long internal ducts.

Deflectors (reference 2) were investigated on only the inlets with divergent ramp walls. Coordinates and photographs of the deflectors installed on the model are shown in figures 6 and 7, respectively. The normal deflectors were tested at both the forward and aft locations of the inlets while various modifications were investigated for the forward location of the inlets.

#### TEST METHODS AND REDUCTION OF DATA

The quantity of air flow through the submerged air inlets of the model was varied and controlled by a centrifugal pump located outside of the wind tunnel. The pump was connected to the duct system by a pipe attached to the rear of the model. The length of the pipe (fig. 2) attached to the model and passing through the wind-tunnel floor was flexible to allow the angle of attack of the model to be changed. A standard sharp-edged ASME orifice meter was used to measure the quantity of air drawn through the submerged air inlets. In determining the inlet velocity ratio from the measured quantity of flow, the free-stream air density was used. This introduced a maximum error of 2.0 percent in the inlet velocity ratio.

Ram pressure recovery, at the duct inlets and at the simulated entrance to the compressor, was measured by rakes of pressure tubes. There were 36 total-pressure and 5 static-pressure tubes in each inlet and 40 total-pressure and 4 static-pressure tubes at the simulated entrance to the compressor. In computing the mean ram recovery ratio at the inlets  $H_1-p_0/H_0-p_0$  the reading of each tube was weighted (reference 2) in accordance with the variation of the mass flow across the duct inlets. As the variations in the velocity were small at the simulated entrance to the compressor, an

arithmetical mean of the tube readings was used to determine the ram recovery ratio  $H_2-p_0/H_0-p_0$  at this position.

The external drag of the submerged inlets was determined for only the forward location of the inlets. Two methods were used to determine the drag: (1) force measurements on the complete model, and (2) measurements of the momentum of the air just behind the inlet location. The force-test drag was measured with the flexible pipe (fig. 2) at the aft of the fuselage removed (fig. 8) while air was allowed to bleed through the internal ducting system. The inlet velocity ratio  $V_1/V_0$  was changed by varying the outlet area  $A_3$  of the duct for the force-test drag measurements.

The drag attributed to the submerged inlets was taken as the difference in the drag, measured by the wind-tunnel balances, with the duct entrances installed and removed less the internal drag. The internal drag was calculated from the loss of momentum per unit time of the air flowing through the internal ducting. The internal drag coefficient was computed with the following equation:

$$C_{D_{\text{internal}}} = \frac{2A_1}{S} \left( \frac{V_1}{V_0} \right) \left[ 1 - \left( \frac{V_1}{V_0} \right) \left( \frac{A_1}{A_3} \right) \left( 1 + \frac{n^2}{1+2n} \right) \right]$$

The value of the constant  $n$  was found to be  $0.44 \times (A_1/A_3)$  from surveys made at the duct exit. The derivation of this equation is presented in Appendix B.

In the determination of the external drag of the submerged entrances by the momentum method, pressure rakes were mounted on the fuselage 3 inches behind the duct lips. The data obtained from the rakes were reduced to drag-coefficient form in a manner similar to that described in Appendix B of reference 2. The drag forces so computed are equal to the change in momentum per unit time at the rake location due to the submerged inlets and do not include the ram drag or the effect of the inlets on the flow over the rear portion of the fuselage.

Pressure-distribution tests were made along the center lines of the ramps and the lips. The critical Mach numbers  $M_{cr}$  of the component parts of the duct entrances (ramps, inside and outside of the lips) were estimated from these pressure distributions by the use of the Karman-Tsien method (reference 5). The pressures on the deflectors were not measured.

## RESULTS AND DISCUSSION

It was realized from previous tests (references 1 to 4) that a thick boundary layer on the fuselage has a detrimental effect on the ram recovery in submerged inlets and that the interference and pressure field of the wing might also be adverse. To determine these effects two locations of the inlets were tested, the forward location where the duct inlets were forward of the wing (fig. 7), and the aft location where the duct inlets were above the point of maximum thickness of the wing (fig. 7).

Figure 9 shows the boundary-layer thickness and the pressure distribution for the two locations measured on the basic fuselage along the fuselage reference plane. The boundary-layer thickness denoted by the parameter  $h/B$  (reference 2) was approximately 1.33 times greater for the aft than for the forward location of the submerged entrances. The efficiencies of the ducting systems evaluated during the bench tests of the long internal ducting and the short internal ducting are shown in figure 10. The efficiency of the short internal ducting was 19 percent higher than that of the long internal ducting.

It was assumed that the airplane represented was powered by a typical gas turbine delivering approximately 3300 shaft horsepower for take-off. The submerged inlets were designed so that the inlet velocity ratio with this gas turbine would be 0.60 at 550 miles per hour and 1.00 in a climb at 350 miles per hour.

## Ram Recovery Ratio

The mean ram recovery ratios at the duct inlets and at the simulated entrance to the compressor are presented in figures 11 to 17 as a function of the model angle of attack and the inlet velocity ratio.

The ram recovery ratio at the inlets is shown in figures 11 and 12 for the forward and aft locations of the submerged entrances, respectively. The effect of angle of attack on the ram recovery in the normal operation range ( $V_1/V_0 = 0.6$  to 1.0) was small. With deflectors on the diverging ramp walls, the ram recovery decreased approximately 0.001 per degree angle of attack and for parallel and diverging ramp walls without deflectors about 0.005 per degree. Figure 13 (obtained from the data of figs. 11 and 12) summarizes the effect of the location of the duct inlets on the entrance ram recovery at  $0^\circ$  angle of attack. The following table compares

these data for an inlet velocity ratio of 0.7:

Forward location		Aft location	
Inlet	$\frac{H_1 - p_0}{H_0 - p_0}$	Inlet	$\frac{H_1 - p_0}{H_0 - p_0}$
Parallel walls	0.890	Parallel walls	0.820
Divergent walls	.970	Divergent walls	.935
Divergent walls with normal deflectors ex- tended forward	.960	Divergent walls with normal deflectors	.940

The differences in the ram recovery between the forward and aft locations of the submerged air inlets were not great. It is believed that the difference in the ram recovery ratios for the two locations was due, primarily, to the difference in the fuselage boundary-layer thickness (fig. 7). It should be noted that identical deflectors were not used in the comparison. Preliminary test data indicated that the forward extension of the deflectors for the front location of the inlets improved the ram recovery for inlet velocity ratios less than 0.7 and produced no effect for higher values. Modification of the deflectors for the aft inlets effected no improvement in the characteristics over those for normal deflectors.

The ram recovery at the simulated face of the compressor is presented in figures 14 to 16 for the forward (long and short internal ducting) and the aft (short internal ducting) locations of the submerged entrances. The effect of angle of attack on the ram recovery ratio at the simulated face of the compressor was similar to that at the entrances. Figure 17 summarizes the data of figures 14 to 16 and shows the effect of the entrance location and of the efficiency  $\eta_D$  of the internal ducting at  $0^\circ$  angle of attack. The following table compares these data for an inlet-velocity ratio of 0.7:

Forward location			Aft location	
Inlet	$\frac{H_2 - P_0}{H_0 - P_0}$		Inlet	$\frac{H_2 - P_0}{H_0 - P_0}$
	Short internal ducting	Long internal ducting		Short internal ducting
Parallel walls	0.780	0.740	Parallel walls	0.670
Divergent walls	.885	.820	Divergent walls	.860
Divergent walls with normal deflectors extended forward	.900	.840	Divergent walls with normal deflectors	.865

The effect of location of the inlets is shown by comparing the data in the above table for the forward and aft locations of the submerged air inlets with the short internal ducting. The difference in ram recovery ratio at the simulated entrance to the compressor due to the location of the inlets was of the same order of magnitude as was measured at the inlets, the forward location having the higher recoveries. However, figure 17 shows that for the divergent-walled entrances with deflectors, a larger ram recovery was obtained for the aft than for the forward location of the inlets, with inlet velocity ratios in excess of 0.9. This difference may be accounted for by a small change in the efficiency  $\eta_D$  of the internal ducting.

The effect of the internal ducting efficiency  $\eta_D$  (fig. 10) may be shown by comparing the data in the preceding table and figure 17 for the forward location of the inlets with the short and long internal ducting. There was only a small difference in the recoveries for inlet velocity ratios below 0.5, but the ram recovery ratio progressively decreased above this value for the longer internal ducting. For an inlet velocity ratio of 1.0 the recoveries at the compressor were reduced 15 to 18 percent below those for the shorter internal ducting.

For inlet velocity ratios greater than 0.65 and 0.83, with divergent and parallel walls, respectively, the ram recoveries at the simulated entrance to the compressor were higher for the aft location of the inlets with the short internal ducting than for

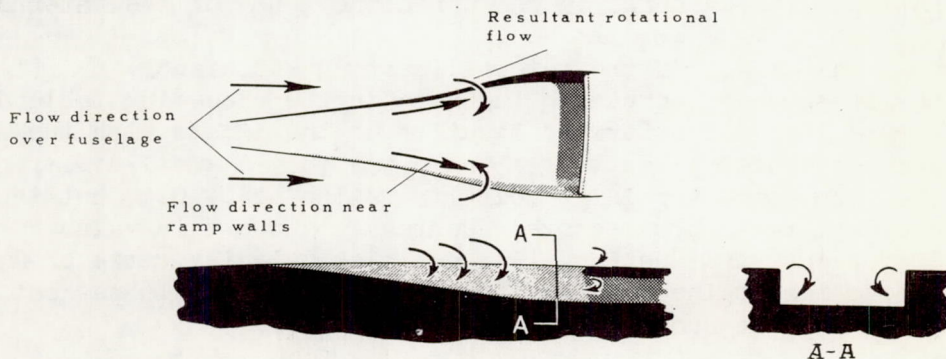
the forward location with the long internal ducting. Consequently, if the location of the compressor is such that long internal ducting must be used for the forward inlets, it might be advantageous to use the aft location of the inlets with the shorter, more efficient, internal ducting system. None of the combinations of the parallel-walled entries and the internal ducting systems give as high a ram recovery at the simulated entrance to the compressor, for high-speed flight, as the poorest combination of the divergent-walled entries and the internal ducting systems investigated.

### Flow Studies

When the entrance ram recovery was measured in the inlets with the diverging ramp walls, two symmetrically located regions of low-velocity air were noted as shown in the sketch.



In an attempt to clarify this phenomenon, visual tuft tests and total-pressure measurements were made. These observations indicated that the air flowing along the ramp followed the divergent walls, while the air flow along the fuselage was approximately parallel to the free stream. Consequently, at the top of the ramp walls there was a discontinuity in the direction of air flow. This discontinuity apparently resulted in a rotational flow as shown below.



From the foregoing discussion it may be conjectured that a part of the fuselage boundary layer developed ahead of the inlets was entrained in the region of rotational flow. Part of the air in the rotational flow passed over the outside of the entrance lips and the remainder entered the ducts, the proportions depending on the operating

conditions of the inlets. For higher inlet velocity ratios the strength of the rotational flow and the proportion that flowed into the entrances increased. This hypothesis appears to explain, qualitatively, the origin of a large portion of the entrance losses encountered with the submerged inlets with divergent ramp walls. For the parallel-walled ramps this rotational flow was less evident, and the major portion of the boundary layer developed ahead of the inlets flowed into the ducts.

### Drag

The external drag coefficients of the NACA submerged inlets as determined from measurements of the change in momentum immediately behind the duct entrances are presented in figure 18. The drag was determined for only the forward location of the duct entrances as the close proximity of the wing made it impossible to install the momentum rakes behind the aft duct entrances. The drag of the entrances with parallel or divergent walls, as indicated by the momentum method, was approximately zero (less than  $C_{Dp} = 0.0001$  based on wing area) for an inlet velocity ratio of 0.7 and  $0^\circ$  angle of attack. For the same condition, the deflectors increased the drag coefficient by approximately 0.0007 based on the wing area. The increase in the drag due to the deflectors appeared to offset the gain in performance due to increased ram recovery (1 percent during high-speed flight) that may be obtained by their use.

The evaluation of the drag increments due to the submerged inlets, by the momentum-survey method, was difficult and time consuming when, as in this test, the surveys were made in a region of three-dimensional flow. In an attempt to verify rapidly the magnitudes of the drag of the submerged inlets measured by the momentum method, data were obtained using the wind-tunnel balance. These data are shown in figure 19. The differences in drag, as measured by the wind-tunnel balance, between the various inlets at a given inlet velocity ratio are considered accurate. However, the absolute values of the drag due to the inlets, as indicated by the wind-tunnel balance measurements, should be considered only qualitative because of the change in the pressure drag of the fuselage with changing exit conditions.

The two methods show fair agreement in the value of  $V_1/V_0$  for which the drag increment was zero for the entrances with divergent walls without deflectors and for those with parallel walls (fig. 19). With other inlet velocity ratios the drag increments (both positive and negative) determined from the wind-tunnel

balance measurements were larger than those from the momentum surveys. In the cases where the momentum surveys indicated small negative drags, the wind-tunnel balance showed larger negative drags. This difference in drag can be explained in part by the fact that for the higher inlet velocity ratios the flow on the rearward portion of the fuselage was improved with a consequent reduction in the over-all fuselage drag in excess of that measured immediately behind the submerged inlets. Conversely, the flow over the rearward part of the fuselage deteriorated with the lower inlet velocity ratios. The same reasoning can also explain why a greater drag increment was measured with the wind-tunnel balance than by the momentum method for the normal deflectors extended forward. (For an  $\alpha$  of  $0^\circ$  and a  $V_1/V_0$  of 0.7, the drag-coefficient increment with the normal deflectors extended forward was 0.0015 as determined from the force tests and 0.0007 as determined from the momentum surveys.)

The increments in drag caused by the deflectors (as measured by the wind-tunnel balance) are presented in figure 20. These data show that considerable reduction in the drag of the deflectors may be obtained by altering the aft portions of the deflectors designed from reference 3. It is believed that separation was occurring on the aft portion of the normal deflectors. To relieve the separation, the aft portions of the deflectors were extended (figs. 6 and 7). This extension reduced the deflector drag as much as 40 percent (fig. 20).

#### Predicted Critical Mach Number

The pressure distribution for the forward location of the inlets with the diverging walls is presented in figure 21. The minimum pressure on the ramp occurred approximately 30 percent of the ramp length from its forward end, and this location did not vary with angle of attack from  $-4^\circ$  to  $4^\circ$  or with inlet velocity ratio. The pressure distribution over the forward 35 percent of the ramp did not change with inlet velocity ratio.

The predicted critical Mach numbers for the ramps and lips are presented in figures 22 and 23. These values of the predicted critical Mach number were computed by the Kármán-Tsien method (reference 5) from the measured low-speed pressure distribution. This method is based on the assumption that the flow over the ramps and lips is two-dimensional, which is not strictly correct, as the duct inlets were tested on a three-dimensional body. It is believed, however, that the results are conservative. (See reference 6.)

The data of figures 22 and 23 show that for identical entrance configurations, the predicted critical Mach numbers were higher for the forward location of the inlets than for the aft location at an angle of attack of  $0^\circ$  for inlet velocity ratios from 0.6 to 0.8. This difference was possibly due to the pressure field of the wing, which reduced the pressure on the basic fuselage (fig. 21) in the vicinity of the aft inlets. The effect of increasing the angle of attack was to decrease the predicted critical Mach number. This effect was more pronounced for the aft location where the submerged entrances were in the pressure field of the wing.

In both the forward and the aft locations, the entrances with divergent walls had higher predicted critical Mach numbers than the entrances with parallel walls. The lips of the parallel-walled entrances were the limiting component of that type of inlet for the high-speed flight condition ( $\alpha = 0^\circ$ ,  $V_1/V_0 = 0.6$  to  $0.7$ ). In the high-speed flight condition the entrances with diverging ramp walls had predicted critical Mach numbers on the ramps and the insides of the lips equal to or greater than the plain wing ( $M_{Cr} = 0.76$ ).

#### CONCLUSIONS

The following conclusions are drawn from the results of tests of several submerged inlets in two locations on a 1/4-scale model of a typical fighter airplane:

1. In both locations on the fuselage, the submerged inlets with the ramps having divergent walls provided a high ram recovery at the simulated entrance to the compressor, high predicted critical Mach numbers, and low external drag.
2. The submerged inlets with ramps having parallel walls were less satisfactory than the submerged inlets with ramps having diverging walls.
3. The ram recovery at the duct entrances, for the inlets tested, was higher with the inlets in the forward than in the aft position.
4. The ram recoveries were higher at the simulated entrance to the compressor, with some inlet velocity ratios, for the aft location of the inlets with the short internal ducting than for the forward location with the longer internal ducting.

5. The drag of the fuselage with submerged duct inlets operating with inlet velocity ratios greater than 0.70 was less than the drag of the basic fuselage; however, with inlet velocity ratios below 0.70 there was an appreciable increase in the drag attributable to the inlets.

6. The external drag of the deflectors more than offset the improved ram recovery they provided on this model.

7. For the high-speed flight condition, the predicted critical Mach number of the inlets was higher for the forward location than the aft location.

Ames Aeronautical Laboratory,  
National Advisory Committee for Aeronautics,  
Moffett Field, Calif.

#### REFERENCES

1. Frick, Charles W., Davis, Wallace F., Randall, Lauros M., and Mossman, Emmet A.: An Experimental Investigation of NACA Submerged-Duct Entrances. NACA ACR No. 5I20, 1945.
2. Mossman, Emmet A., and Randall, Lauros M.: An Experimental Investigation of the Design Variables for NACA Submerged Duct Entrances. NACA RM No. A7I30, 1947.
3. Gault, Donald E.: An Experimental Investigation of NACA Submerged Air Inlets on a 1/5-Scale Model of a Fighter Airplane. NACA RM No. A7I06, 1947.
4. Mossman, Emmet A., and Gault, Donald E.: Development of NACA Submerged Inlets and a Comparison with Wing Leading-Edge Inlets for a 1/4-Scale Model of a Fighter Airplane. NACA RM No. A7A31, 1947.
5. von Kármán, Th.: Compressibility Effects in Aerodynamics. Jour. Aero. Sci., vol. 8, no. 9, July 1941, pp. 337-356.
6. Lees, Lester: A Discussion of the Application of the Prandtl-Glauert Method to Subsonic Compressible Flow Over a Slender Body of Revolution. NACA TN No. 1127, 1946.

APPENDIX A

PERTINENT DIMENSIONS OF THE 1/4-SCALE MODEL  
OF A TYPICAL FIGHTER-TYPE AIRPLANE

Model

Wing area . . . . .	14.519 sq ft
Aspect ratio . . . . .	4.98
Wing span . . . . .	8.50 ft
Wing section . . . . .	63 <sub>1</sub> -110
Root chord . . . . .	2.30 ft
Tip chord . . . . .	1.15 ft
Wing incidence . . . . .	0°

Submerged Inlets

Ramp angle . . . . .	7°
Aspect ratio of inlet . . . . .	4
Total cross-sectional area of both inlets measured 1½ inches behind lip leading edges . . . . .	0.0718 sq ft
Depth of the ramps at the lip leading edges . . . . .	1.720 in.
Distance of duct-lip leading edges from wing leading edge	
Forward location . . . . .	19.3 percent root chord ahead
Aft location . . . . .	35.6 percent root chord behind
Distance of inlet center lines above the wing at the fuselage juncture . . . . .	7.1 percent root chord

Length of the internal duct from lip leading edge  
to the simulated entrance of the compressor

Short internal ducting . . . . .	15.25 in.
Long internal ducting . . . . .	29.5 in.
Area ratio $\left(\frac{A_2}{A_1}\right)$ . . . . .	1.336

#### APPENDIX B

##### Determination of Internal Drag

For the determination of the external drag of the twin submerged duct inlets the drag of the internal ducting had to be determined. The internal drag was computed from the inlet velocity ratio  $V_1/V_0$ , wing area  $S$ , duct inlet area  $A_1$ , and the duct exit area  $A_3$ .

The internal drag was taken as the free-stream ram drag minus the momentum of the air per unit time exiting from the tail pipe (reference 2).

$$C_{D\text{internal}} = \frac{\rho A_1 V_1 V_0}{q_0 S} - \frac{\rho}{q_0 S} \int_0^{R_3} 2\pi r_3 v_3^2 dr_3 \quad (\text{B1})$$

The first term of equation (1) is readily evaluated. For the second term, surveys were made at the exit across one diameter to determine the variation of the velocity  $v_3$  across the outlet. The velocity distribution was assumed equal on all diameters. The experimental velocity profiles were plotted and matched by a mathematical curve

$$\frac{v_3}{v_{3\text{max}}} = \left[ 1 - \left( \frac{r_3}{R_3} \right)^2 \right]^n \quad (\text{B2})$$

where  $n$  was found to be equal to  $0.44 A_1/A_3$ , where  $A_1/A_3$  is the ratio of entrance area to exit area. Using this value of  $n$ , the mathematical curve showed good agreement with the experimental points. If the flow had been laminar, the value of  $n$  would have been one.

The average velocity across the exit is

$$V_3 = \frac{2}{R_3^2} \int_0^{R_3} r_3 v_3 dr_3 \quad (B3)$$

Substituting the value of  $v_3$  from equation (B2) and integrating equation (B3)

$$V_3 = \frac{v_{3\max}}{(1+n)} \quad (B4)$$

From the continuity equation for an incompressible fluid  $V_1 A_1 = V_3 A_3$ . Substituting this in equation (B4)

$$v_{3\max} = V_1 \left( \frac{A_1}{A_3} \right) (1+n) \quad (B5)$$

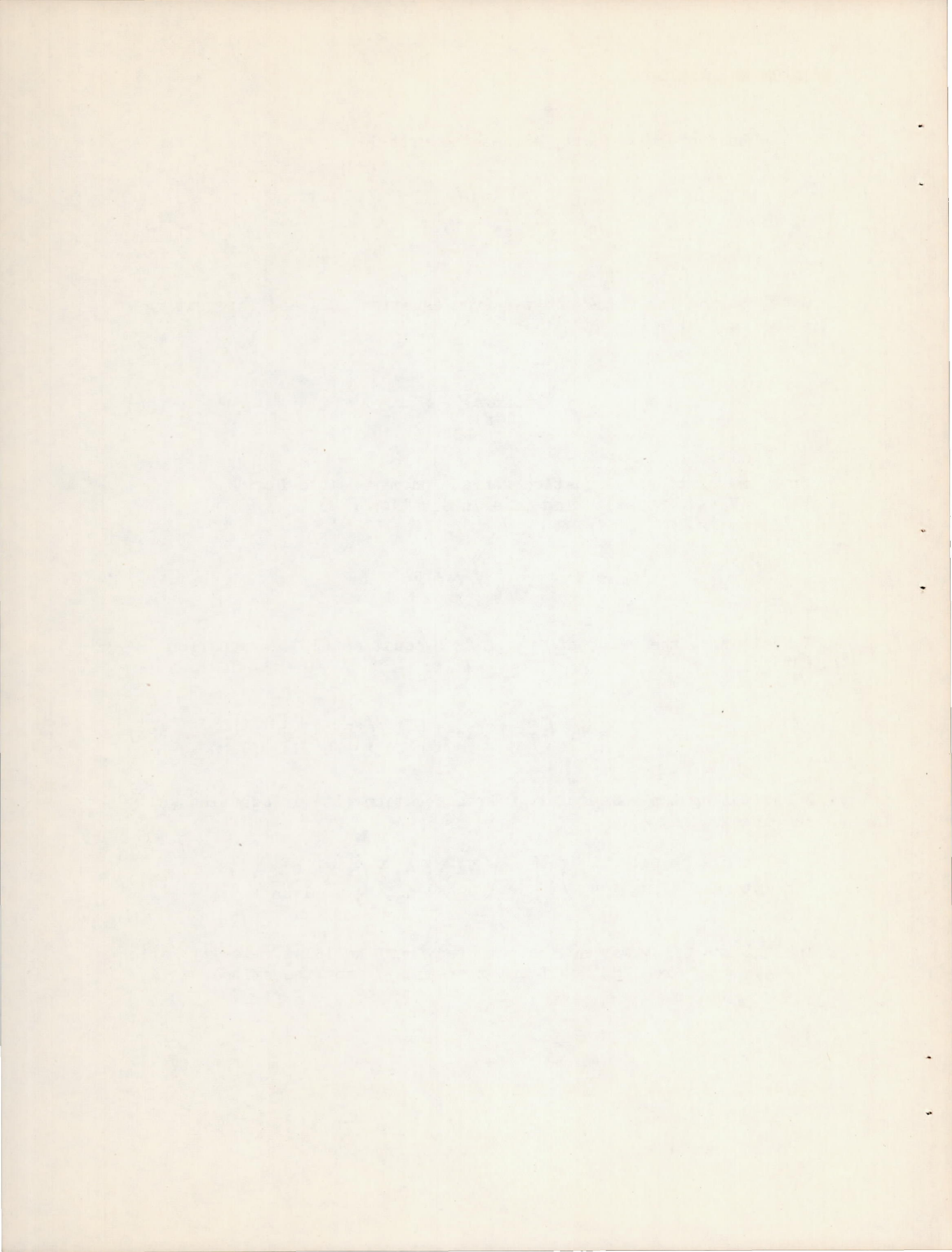
Substituting the value of  $v_{3\max}$  from equation (B5) in equation (B2)

$$v_3 = V_1 \left( \frac{A_1}{A_3} \right) (1+n) \left[ 1 - \left( \frac{r_3}{R_3} \right)^2 \right]^n \quad (B6)$$

Substituting the value of  $v_3$  from equation (B6) in equation (B1) and integrating

$$C_{D\text{internal}} = \frac{2A_1}{S} \left( \frac{V_1}{V_0} \right) \left[ 1 - \left( \frac{V_1}{V_0} \right) \left( \frac{A_1}{A_3} \right) \left( 1 + \frac{n^2}{1+2n} \right) \right] \quad (B7)$$

The internal drag may now be computed from the inlet velocity ratio  $V_1/V_0$ , wing area  $S$ , duct inlet area  $A_1$ , and the exit area  $A_3$ .



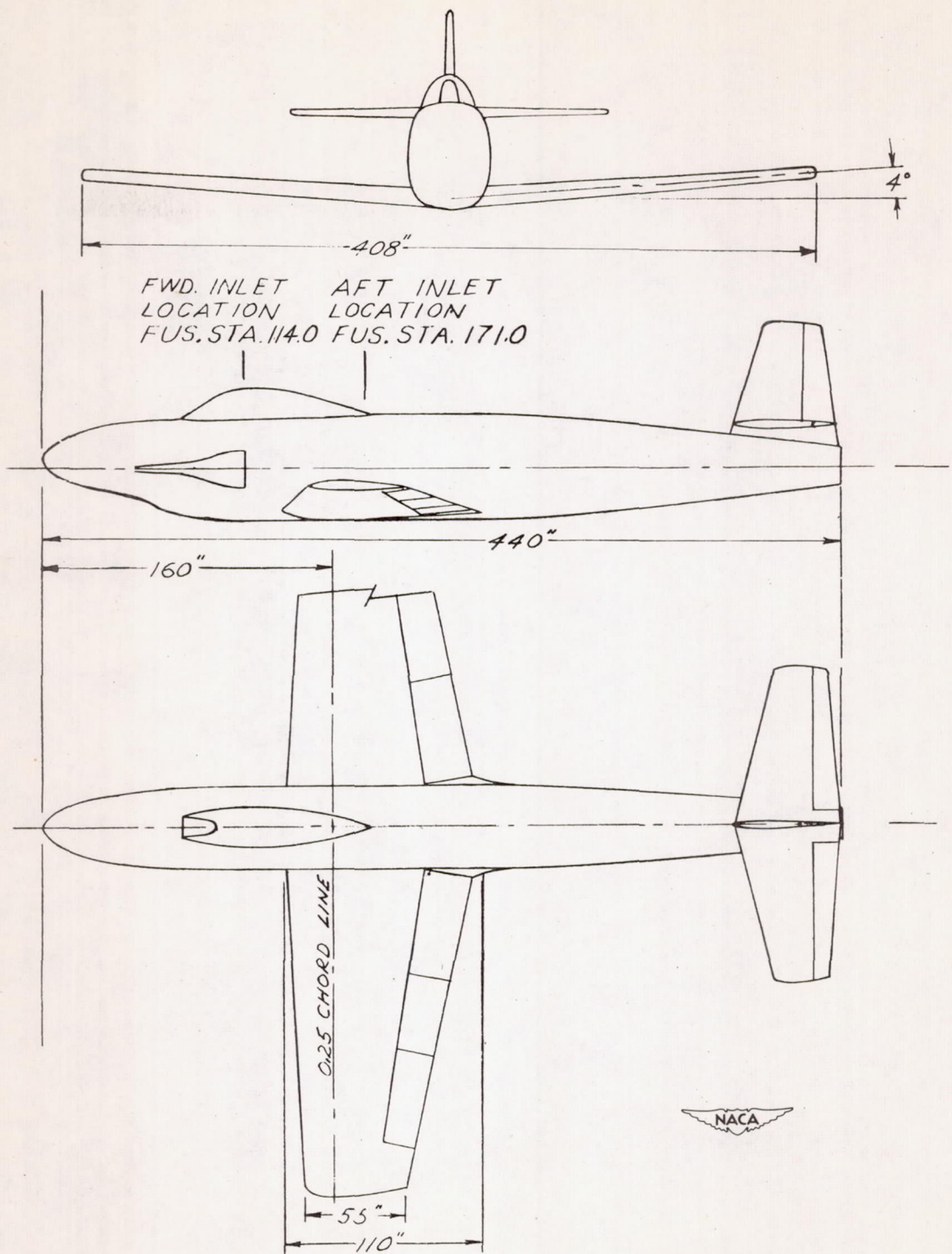


FIGURE 1- A THREE-VIEW DRAWING OF THE AIRPLANE

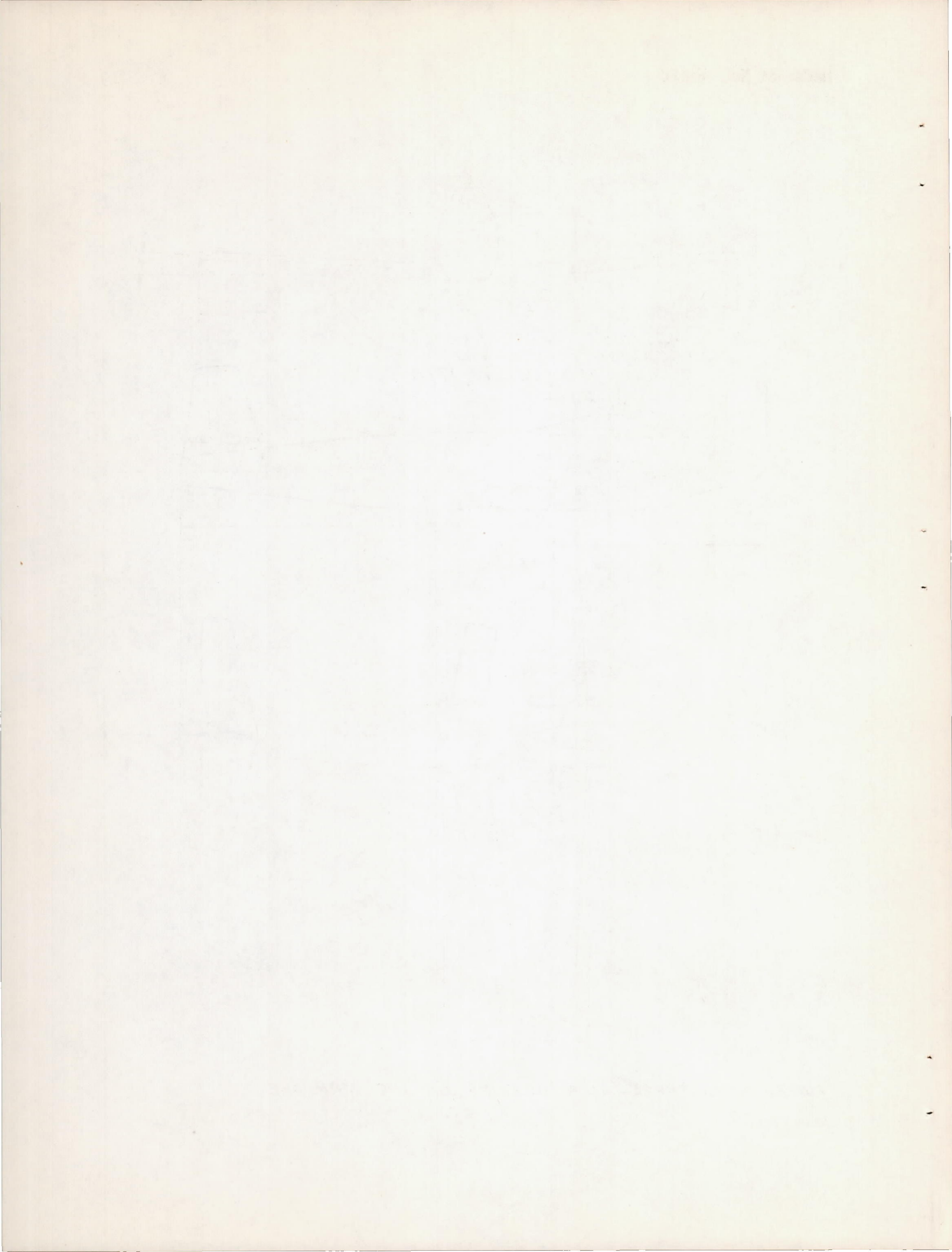
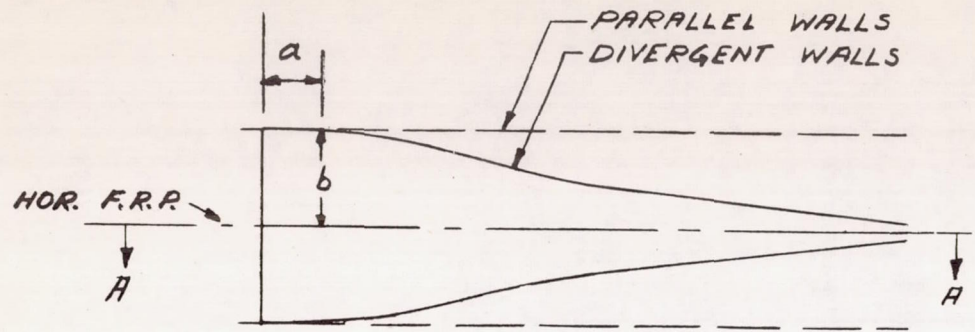


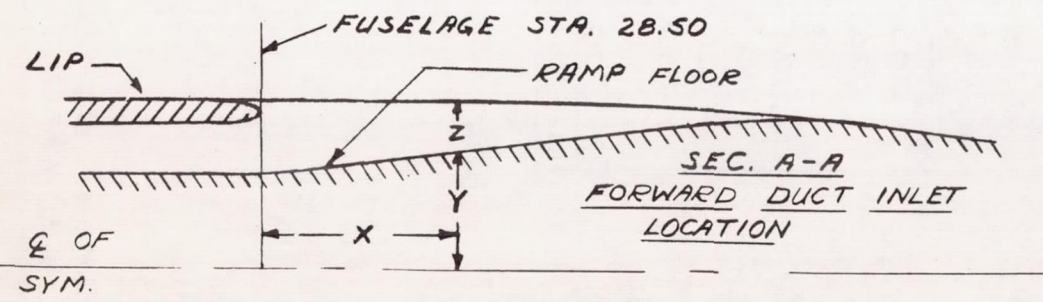
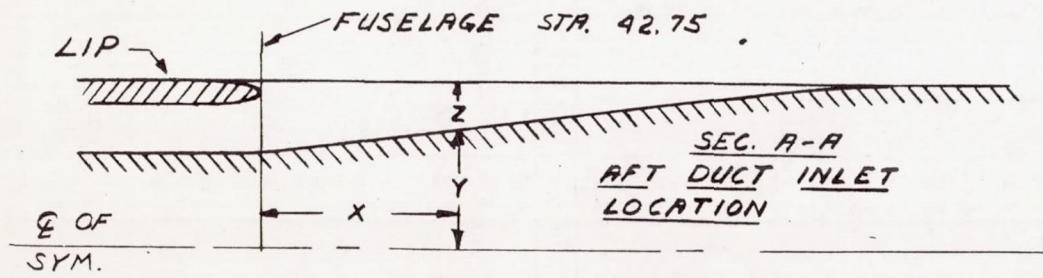


Figure 2.- The 1/4-scale model of a fighter airplane installed in the 7- by 10-foot wind tunnel.





RAMP PLAN FORM



a	b	a	b
0 (LIP)	2.340	9.324	0.913
1.554	2.328	10.878	0.733
3.108	2.141	12.432	0.544
4.662	1.790	13.986	0.374
6.216	1.439	15.540	0.195
7.770	1.120	—	—

X	AFT LOCATION		FORWARD LOCATION	
	Y	Z	Y	Z
-1.00	4.013	5.750	4.013	5.750
0	4.030		4.030	
2.00	4.275		4.270	
4.00	4.517		4.509	5.733
6.00	4.759		4.729	5.710
8.00	5.001		4.936	5.680
10.00	5.243		5.112	5.620
12.00	5.485		5.248	5.512
14.00	5.693		5.298	5.355
14.50	5.723		5.280	5.310
15.54	5.750		5.220	5.220

ALL DIMENSIONS ARE INCHES MODEL SCALE

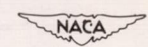
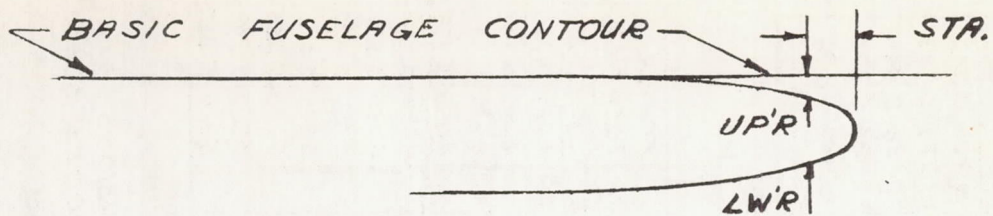


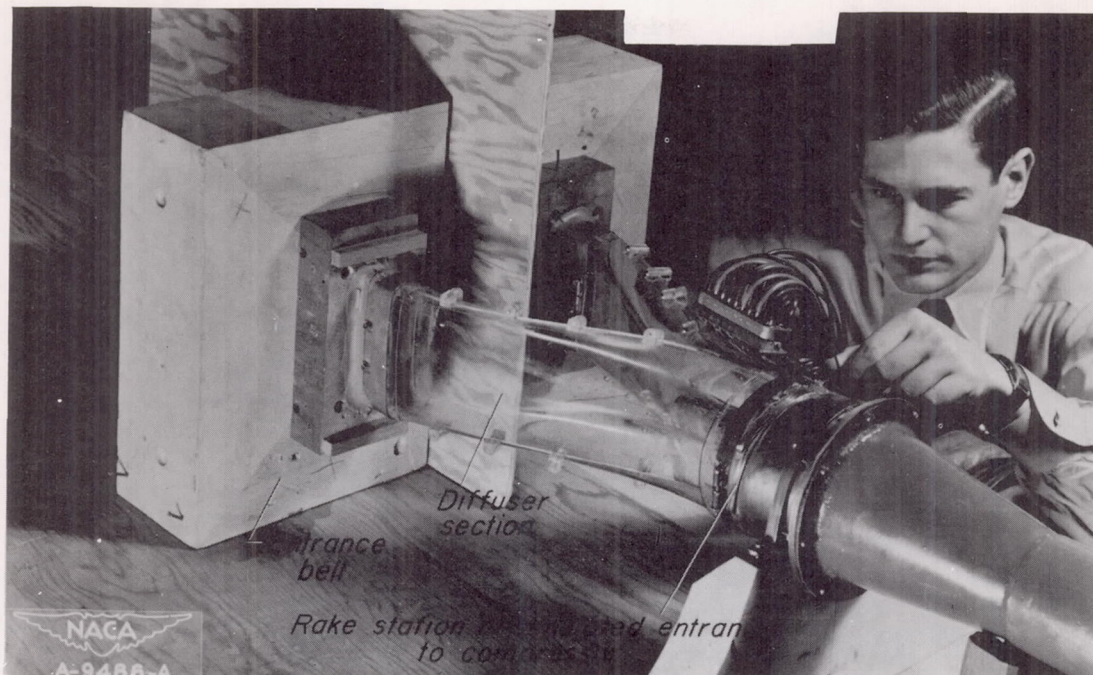
FIGURE 3.- COORDINATES OF THE 7° RAMPS FOR THE SUBMERGED AIR INLETS.



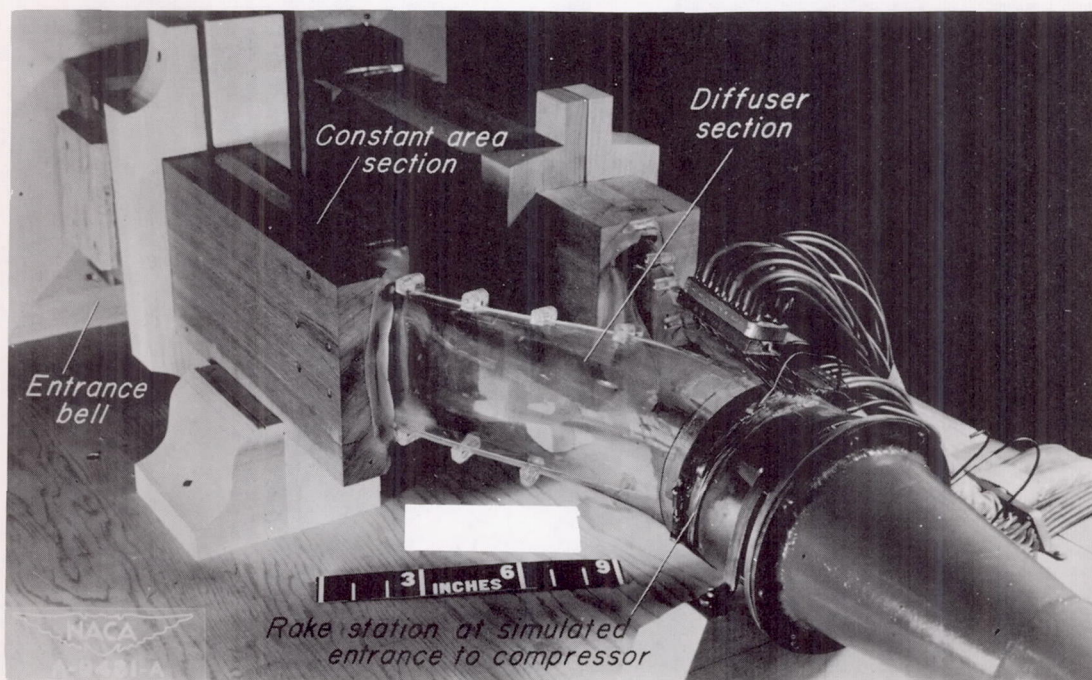
STATION	UPPER (OUTSIDE)	LOWER (INSIDE)
0	0.285	0.285
0.125	.163	.416
.250	.123	.463
.375	.094	.498
.500	.069	.521
.625	.051	.540
.750	.038	.550
.875	.025	.569
1.000	.016	.579
1.125	.009	.588
1.250	.006	.593
1.375	.003	.598
1.500	.000	.600
LEADING EDGE RADIUS = .107		

ALL DIMENSIONS ARE INCHES,  
MODEL SCALE 

FIGURE 4. - COORDINATES OF THE LIPS FOR THE SUBMERGED AIR INLETS.



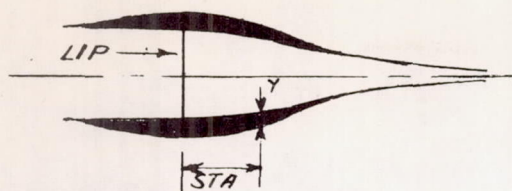
(a) Short internal ducting system.



(b) Long internal ducting system.

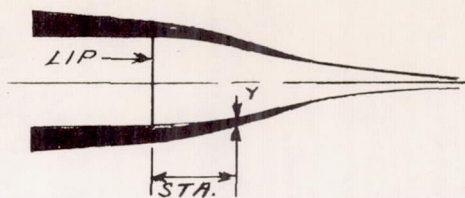
Figure 5.- Bench-test installation of the internal ducting.





DEFLECTORS EXTENDED AFT

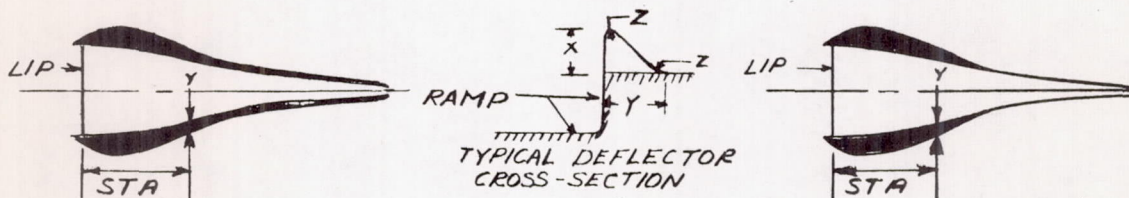
STA	X	Y	STA	X	Y
-6.0	0	0	1.5	.54	.79
-5.5	.03	.04	2.0	.53	.77
-5.0	.08	.12	2.5	.52	.75
-4.5	.15	.20	3.0	.51	.73
-4.0	.21	.30	3.5	.48	.70
-3.5	.27	.39	4.0	.42	.61
-3.0	.33	.48	4.5	.38	.55
-2.5	.38	.55	5.0	.33	.48
-2.0	.42	.61	5.5	.27	.39
-1.5	.48	.70	6.0	.21	.30
-1.0	.51	.73	6.5	.15	.20
-0.5	.52	.75	7.0	.08	.12
0	.53	.77	7.5	.03	.04
0.5	.54	.79	8.0	0	0
1.0	.55	.80			



BEAVER TAIL DEFLECTORS

STA	X	Y	STA	X	Y
-6.0	0	1.25	1.5	.54	.57
-5.5	.03	1.21	2.0	.53	.54
-5.0	.08	1.16	2.5	.52	.49
-4.5	.15	1.12	3.0	.51	.45
-4.0	.21	1.07	3.5	.48	.40
-3.5	.27	1.03	4.0	.42	.36
-3.0	.33	.98	4.5	.38	.31
-2.5	.38	.94	5.0	.33	.27
-2.0	.42	.89	5.5	.27	.22
-1.5	.48	.85	6.0	.21	.18
-1.0	.51	.80	6.5	.15	.13
-0.5	.52	.76	7.0	.08	.09
0	.53	.71	7.5	.03	.04
0.5	.54	.67	8.0	0	0
1.0	.55	.62			

$Z = 0.20 X$



NORMAL DEFLECTORS EXTENDED FORWARD

STA	X	Y	STA	X	Y
-0.5	0	0	4.0	.56	.81
-0.25	.08	.12	4.5	.50	.72
0	.21	.30	5.0	.44	.63
0.5	.47	.68	5.5	.36	.52
1.0	.61	.88	6.0	.28	.40
1.5	.68	.98	6.5	.20	.29
2.0	.70	1.01	7.0	.13	.19
2.5	.69	.99	15.0	.13	.19
3.0	.67	.96	15.25	.12	.17
3.5	.63	.88	15.50	0	0

NORMAL DEFLECTORS

STA	X	Y	STA	X	Y
-0.5	0	0	4.0	.56	.81
-0.25	.08	.12	4.5	.50	.72
0	.21	.30	5.0	.44	.63
0.5	.47	.68	5.5	.36	.52
1.0	.61	.88	6.0	.28	.40
1.5	.68	.98	6.5	.20	.29
2.0	.70	1.01	7.0	.11	.16
2.5	.69	.99	7.5	.04	.06
3.0	.67	.96	8.0	0	0
3.5	.63	.88			

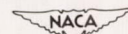
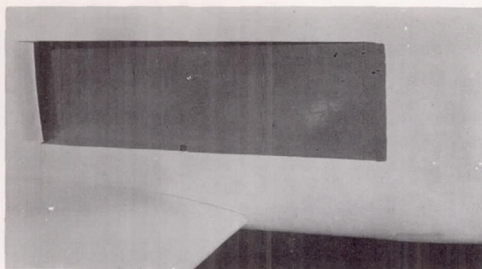
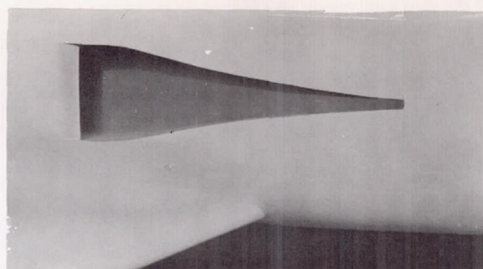


FIGURE 6. - COORDINATES OF THE DEFLECTORS FOR THE SUBMERGED AIR INLETS.

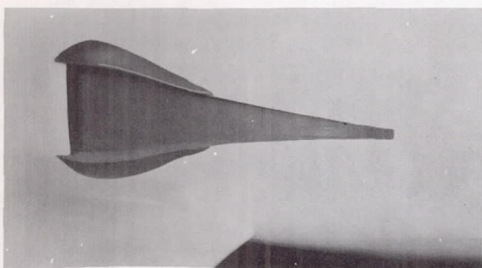




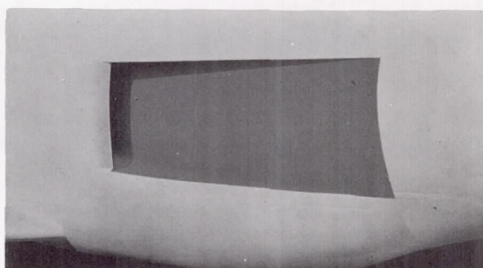
(a) Aft inlet with parallel ramp walls.



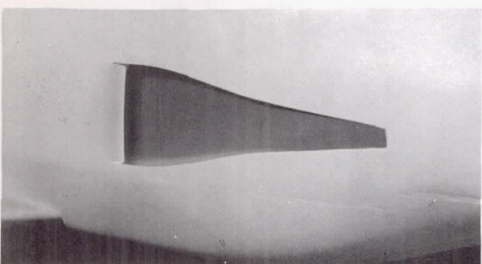
(b) Aft inlet with diverging ramp walls.



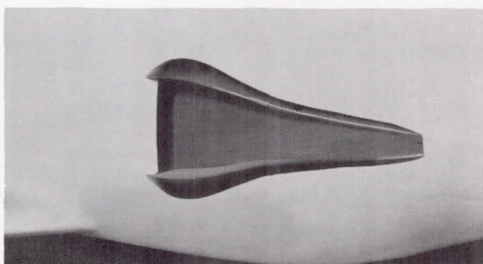
(c) Aft inlet with diverging ramp walls and normal deflectors.



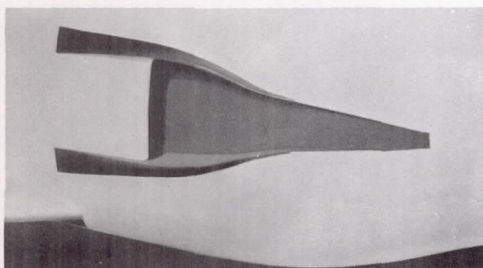
(d) Forward inlet with parallel ramp walls.



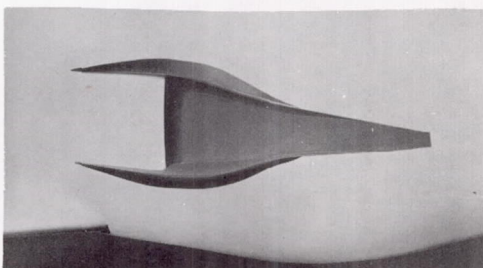
(e) Forward inlet with diverging ramp walls.



(f) Forward inlet with diverging ramp walls and normal deflectors extended forward.



(g) Forward inlet with diverging ramp walls and beaver-tail deflectors.



(h) Forward inlet with diverging ramp walls and deflectors extended aft.

Figure 7.- Pictures of the various submerged air inlets.



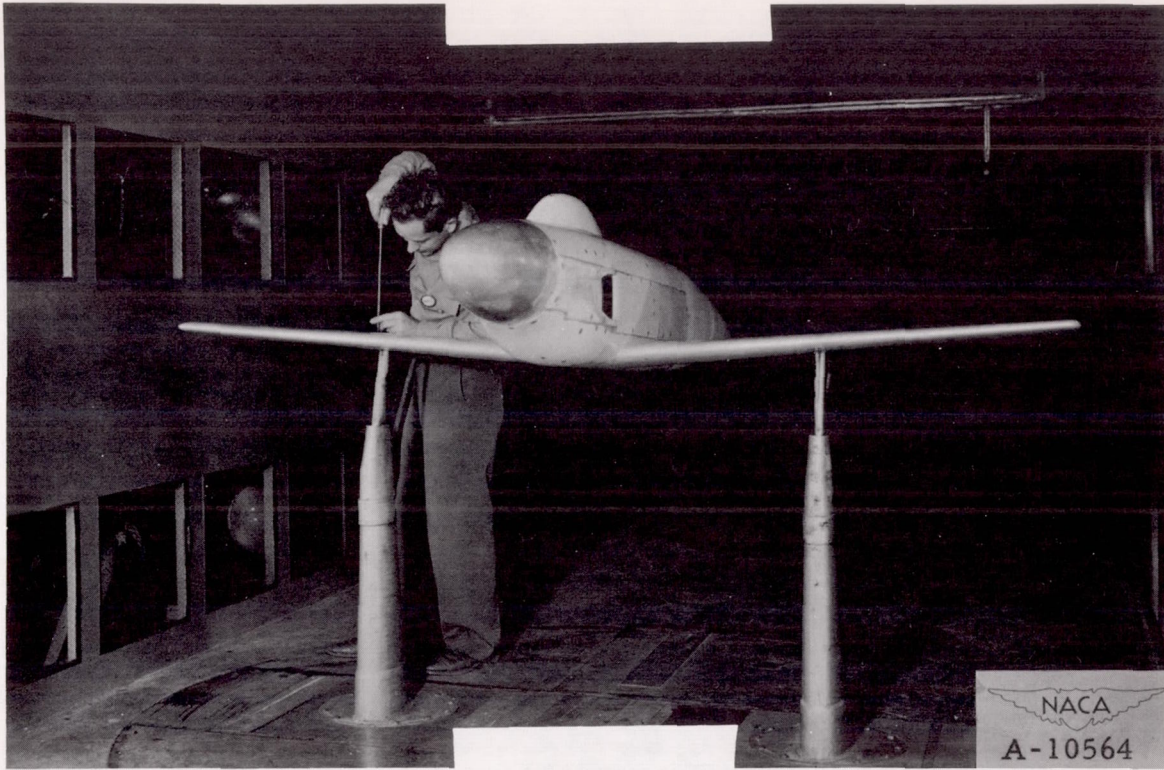


Figure 8.- The 1/4-scale model of the fighter-type airplane installed in the 7- by 10-foot wind tunnel for force-test drag measurements.



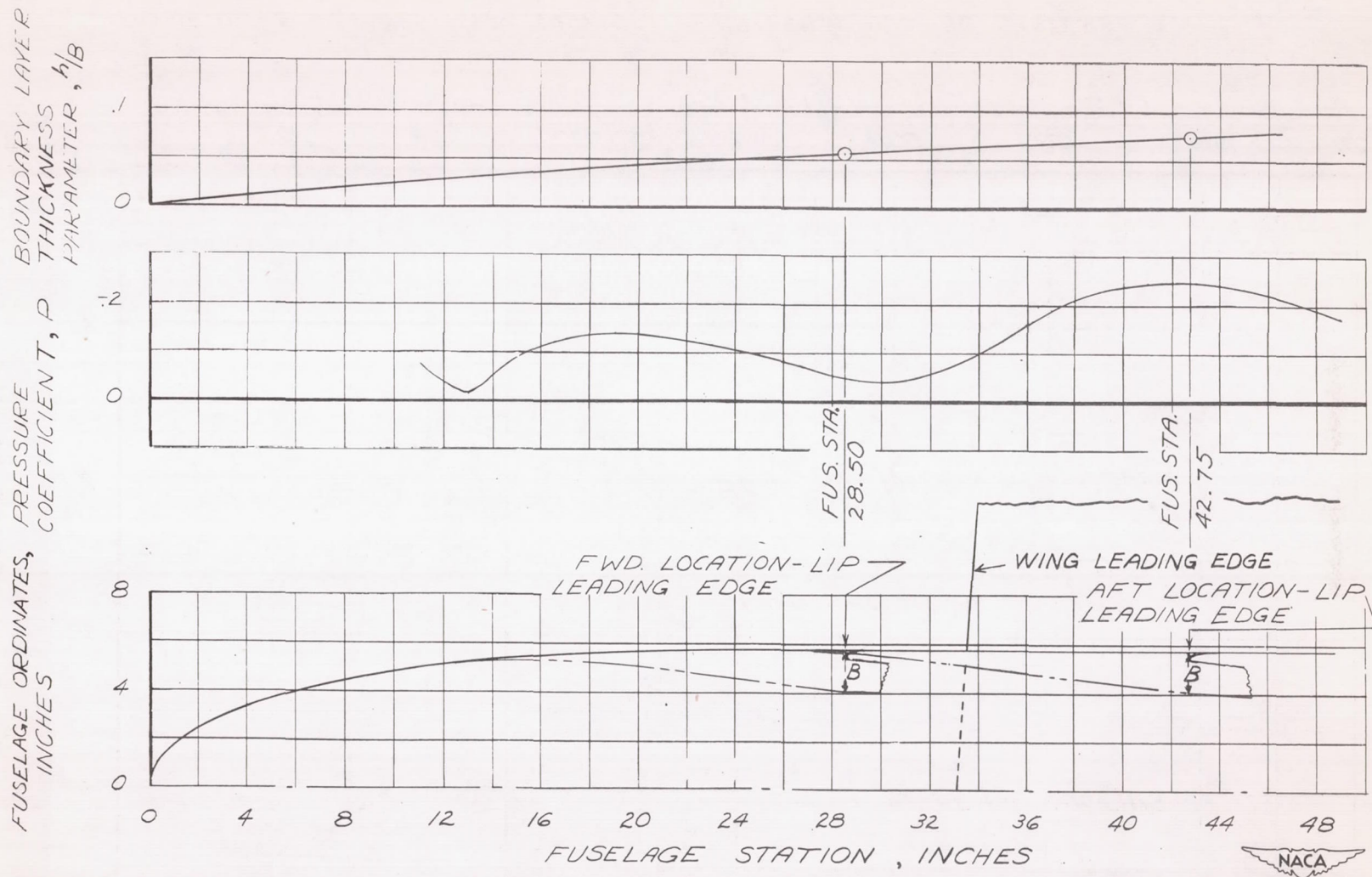


FIGURE 9. - BOUNDARY-LAYER THICKNESS AND PRESSURE DISTRIBUTION ON THE BASIC FUSELAGE MEASURED ON THE CENTER LINE OF THE SUBMERGED AIR INLETS.  $\alpha$ ,  $0.3^\circ$ .

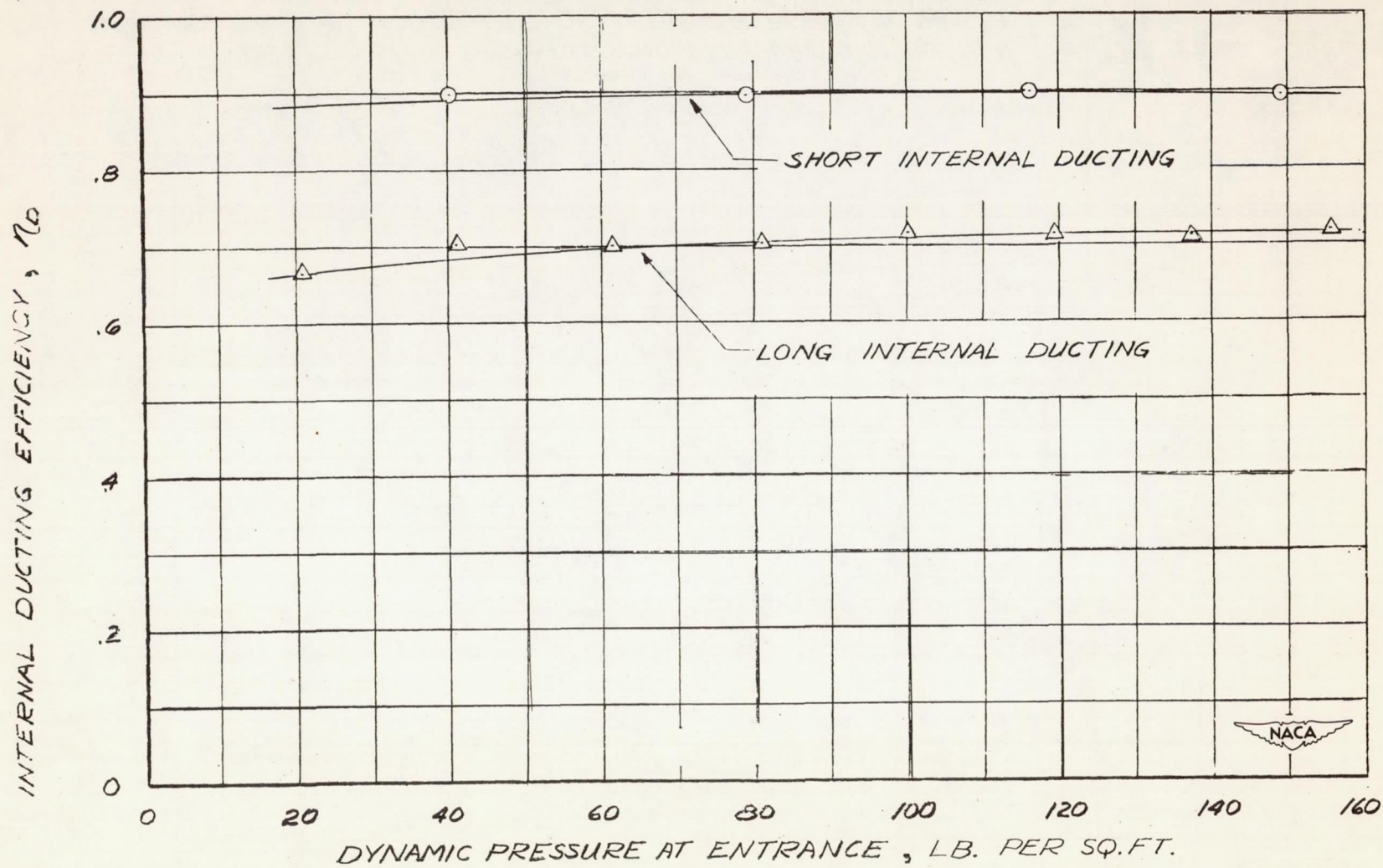


FIGURE 10.- BENCH-TEST EFFICIENCY OF THE INTERNAL DUCTING SYSTEMS.

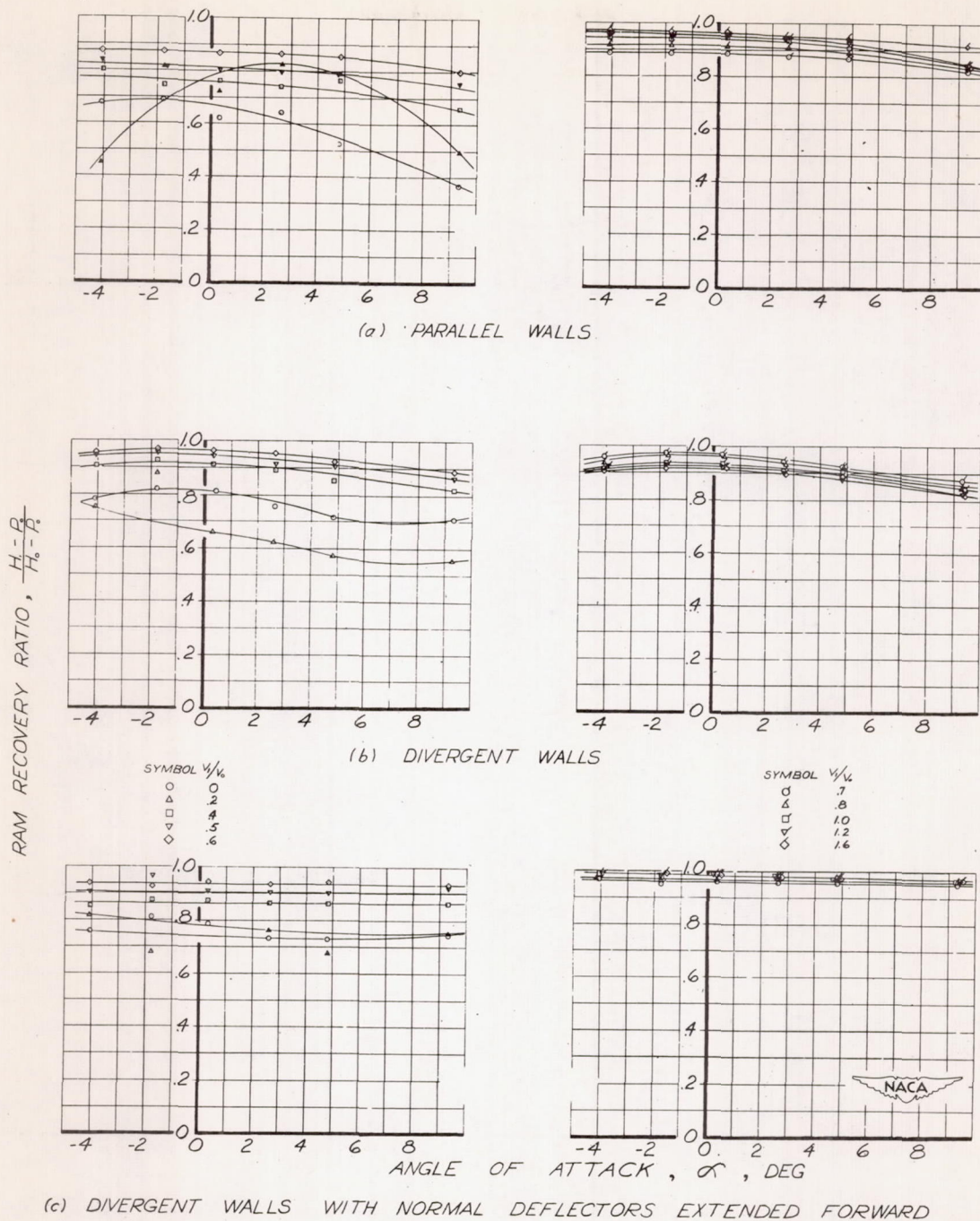
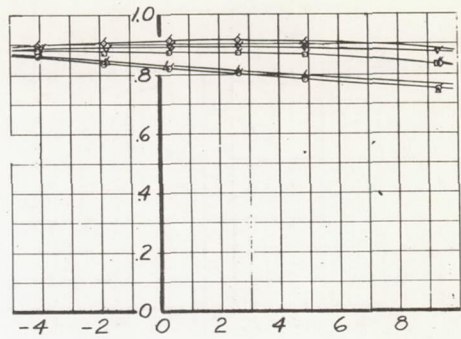
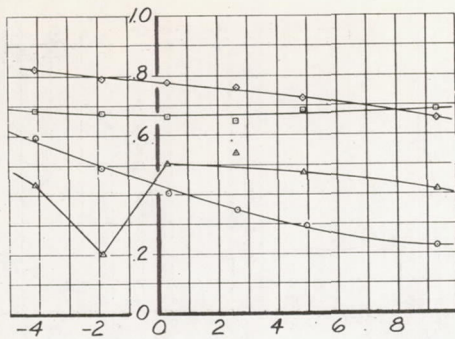
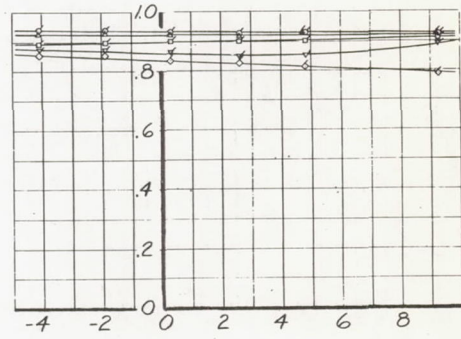
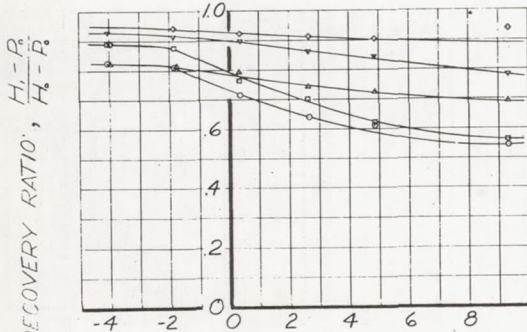


FIGURE 11. - VARIATION OF THE RAM RECOVERY RATIO AT THE INLET WITH ANGLE OF ATTACK FOR THE FORWARD SUBMERGED INLETS.



(a) PARALLEL WALLS



(b) DIVERGENT WALLS

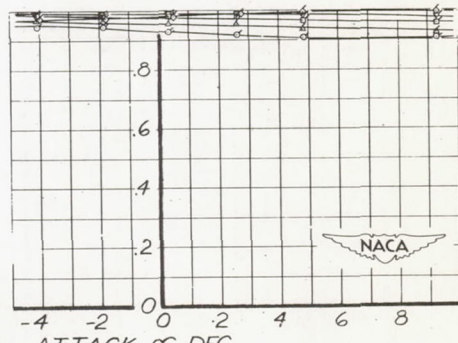
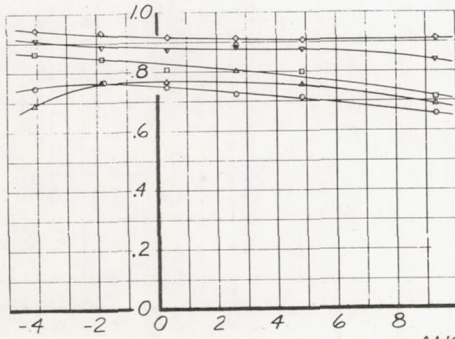
RAM RECOVERY RATIO,  $\frac{H_1 - P_0}{H_2 - P_0}$

SYMBOL  $V/V_0$

- 0
- △ .2
- .4
- ▽ .5
- ◇ .6

SYMBOL  $V/V_0$

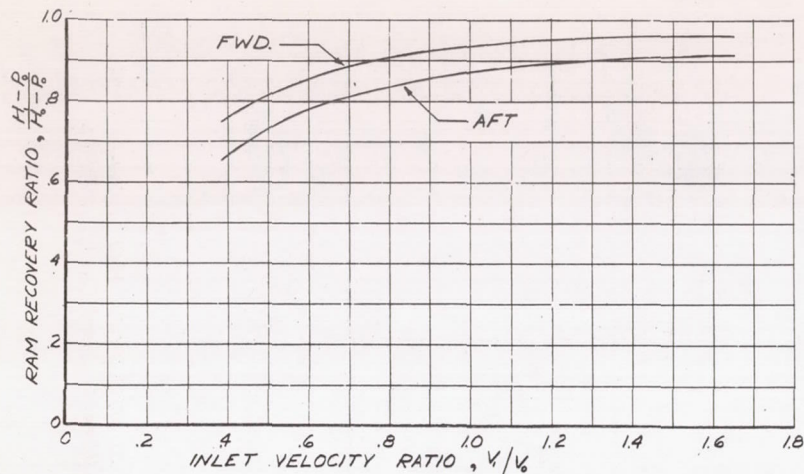
- .7
- △ .8
- 1.0
- ▽ 1.2
- ◇ 1.6



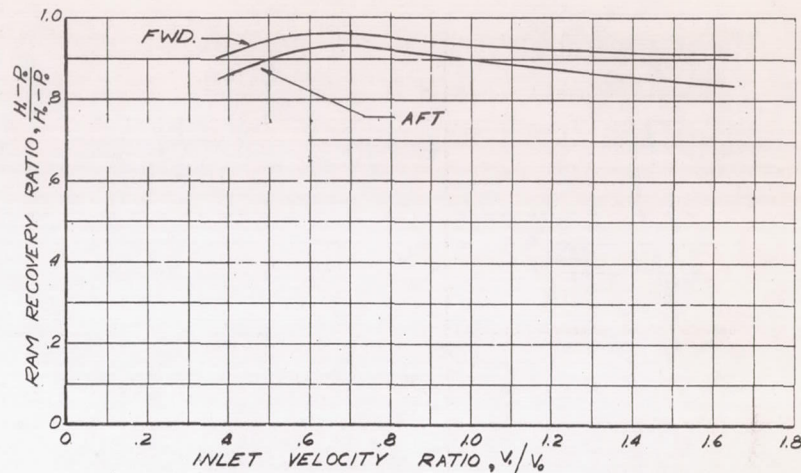
ANGLE OF ATTACK,  $\alpha$ , DEG

(c) DIVERGENT WALLS WITH NORMAL DEFLECTORS

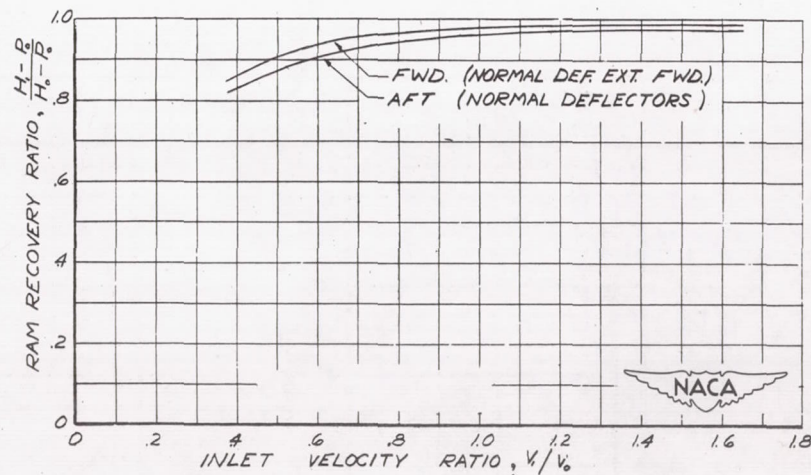
FIGURE 12. - VARIATION OF THE RAM RECOVERY RATIO AT THE INLET WITH ANGLE OF ATTACK FOR THE AFT SUBMERGED INLETS.



(a) PARALLEL WALLS



(b) DIVERGENT WALLS



(c) DIVERGENT WALLS WITH DEFLECTORS

FIGURE 13. - THE EFFECT OF THE LOCATION OF THE INLET ON THE RAM RECOVERY RATIO AT THE INLETS.  $\alpha, 0^\circ$

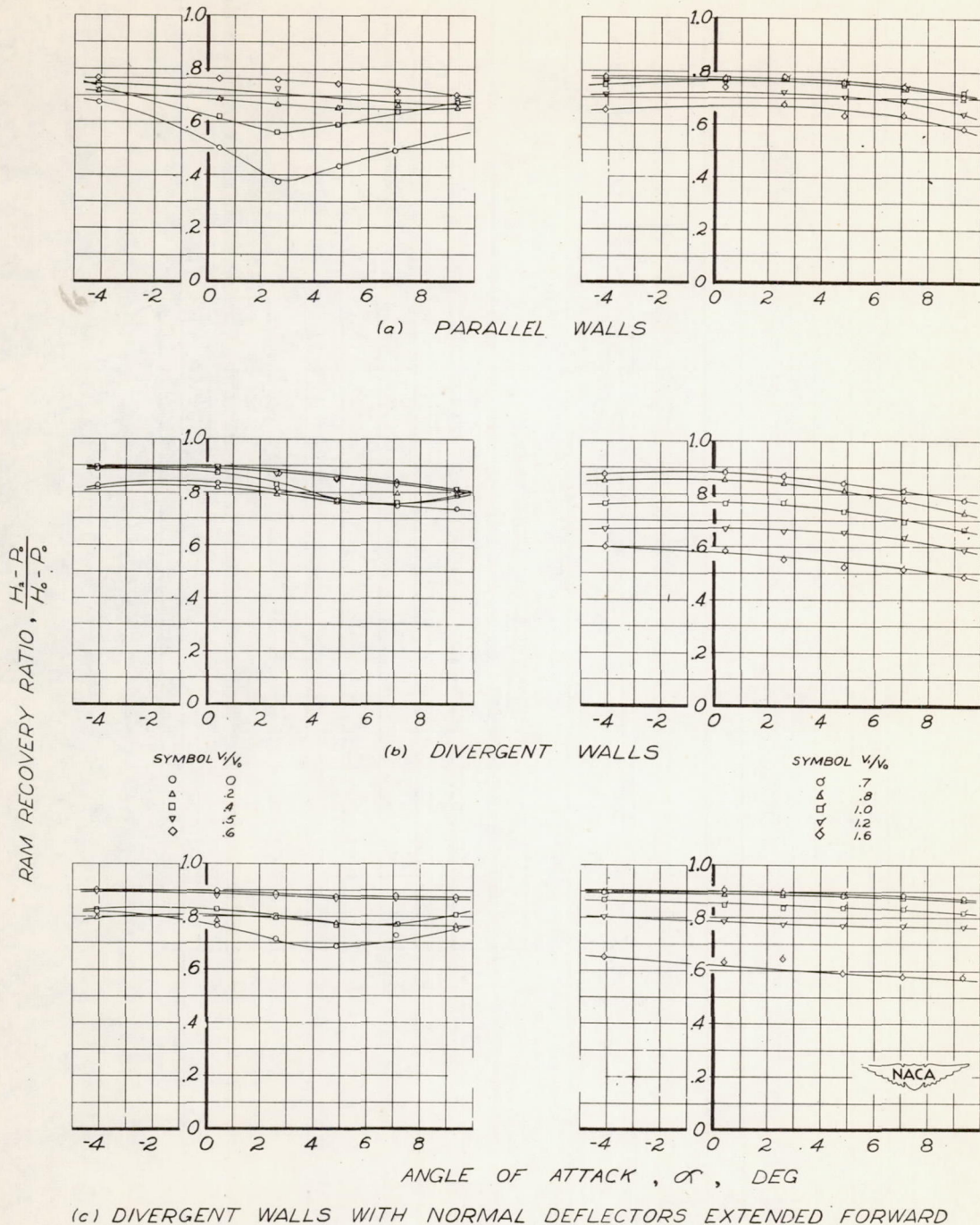
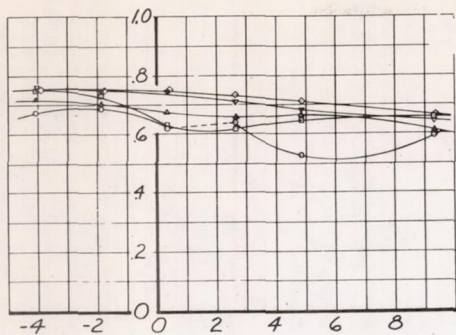
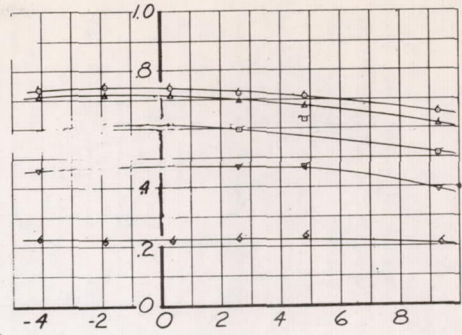


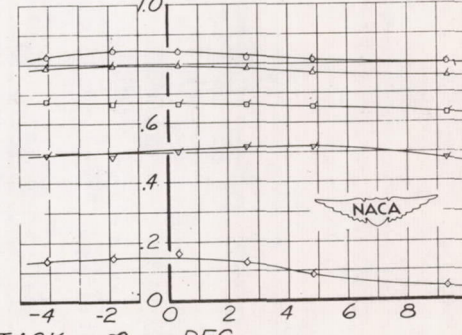
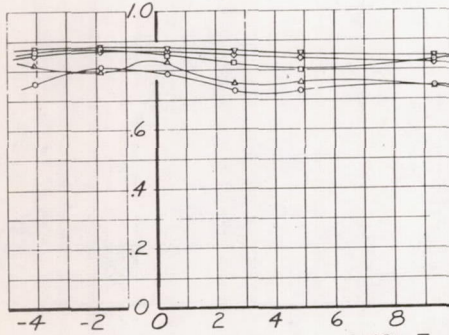
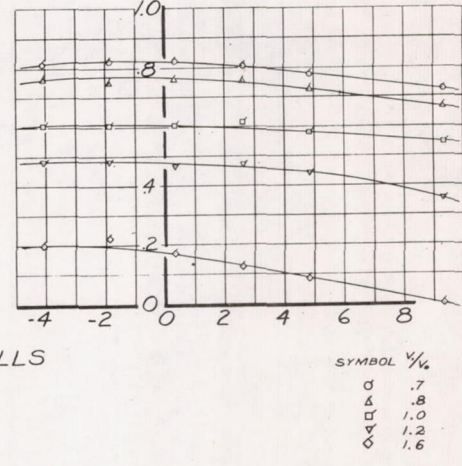
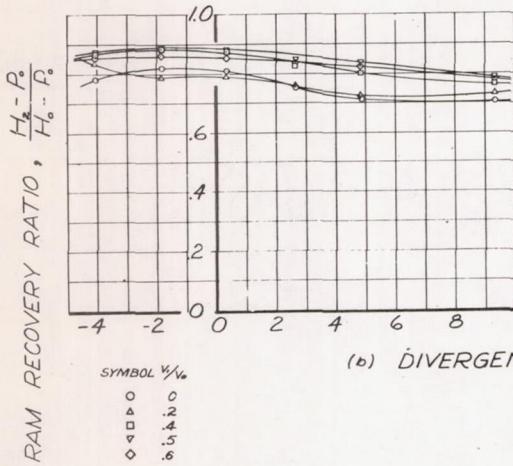
FIGURE 14.- VARIATION OF THE RAM RECOVERY RATIO AT THE SIMULATED COMPRESSOR ENTRANCE WITH ANGLE OF ATTACK FOR THE FORWARD SUBMERGED INLETS. SHORT INTERNAL DUCTING.



(a) PARALLEL WALLS

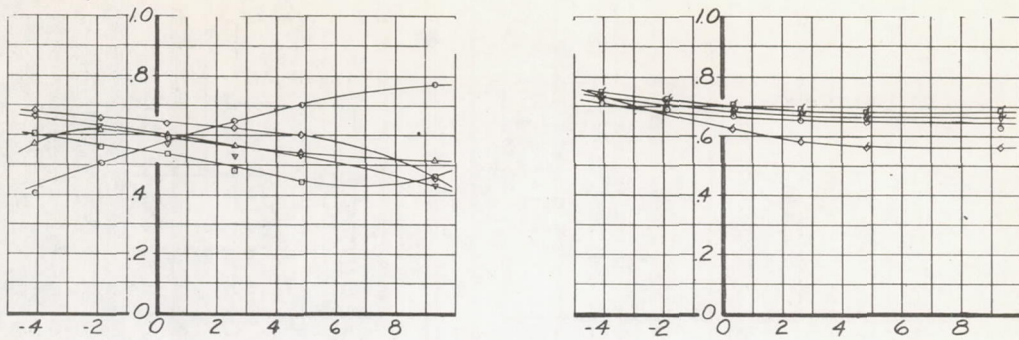


(b) DIVERGENT WALLS

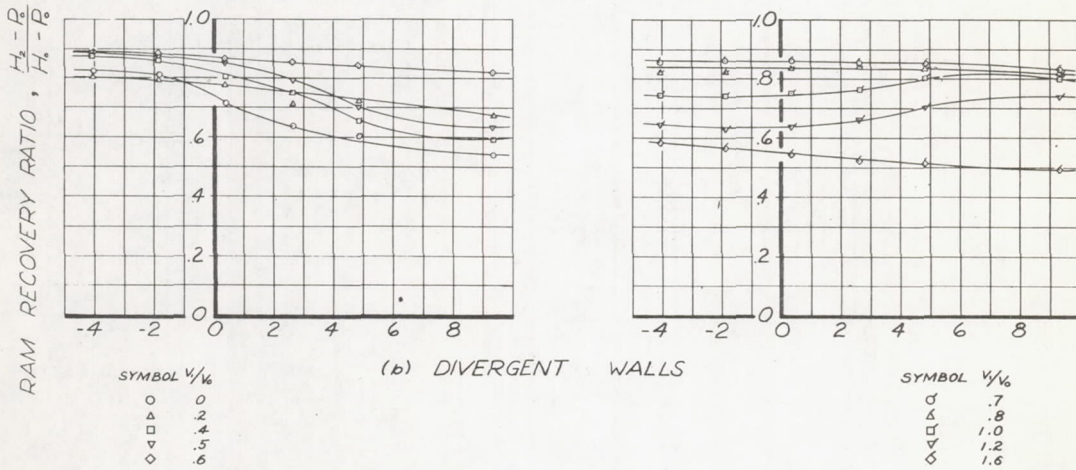


(c) DIVERGENT WALLS WITH NORMAL DEFLECTORS EXTENDED FORWARD

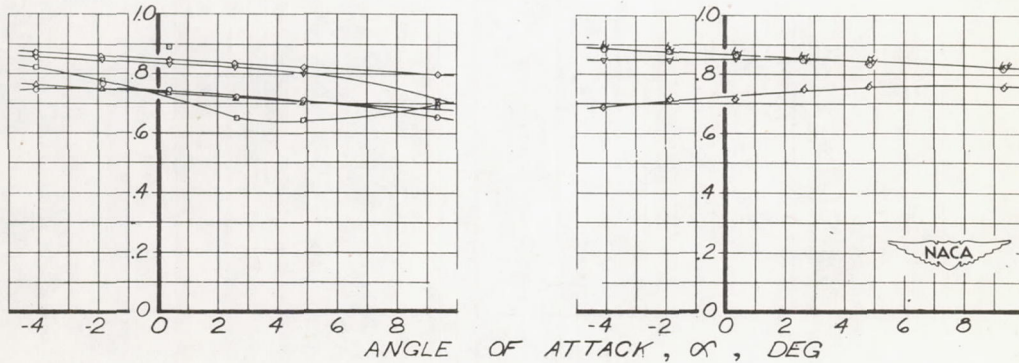
FIGURE 15.- VARIATION OF THE RAM RECOVERY RATIO AT THE SIMULATED COMPRESSOR ENTRANCE WITH ANGLE OF ATTACK FOR THE FORWARD SUBMERGED INLETS. LONG INTERNAL DUCTING.



(a) PARALLEL WALLS

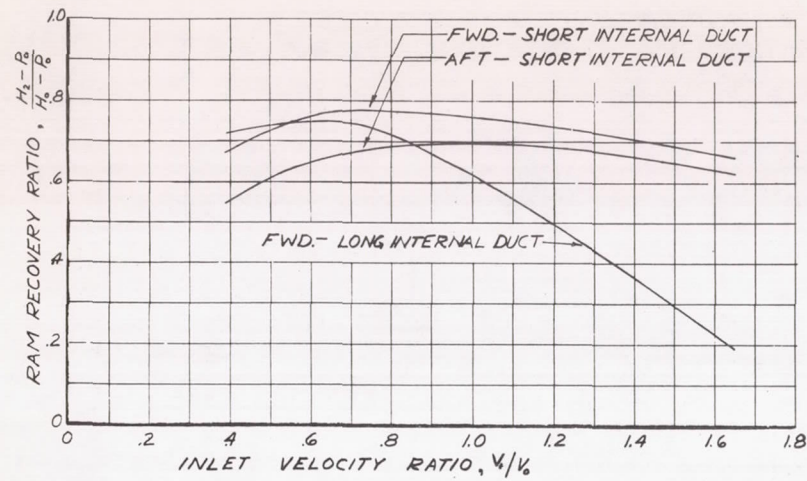


(b) DIVERGENT WALLS

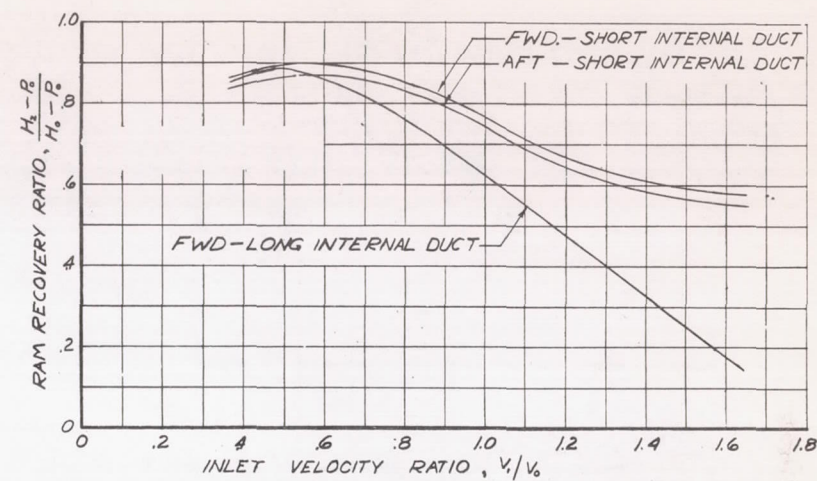


(c) DIVERGENT WALLS WITH NORMAL DEFLECTORS

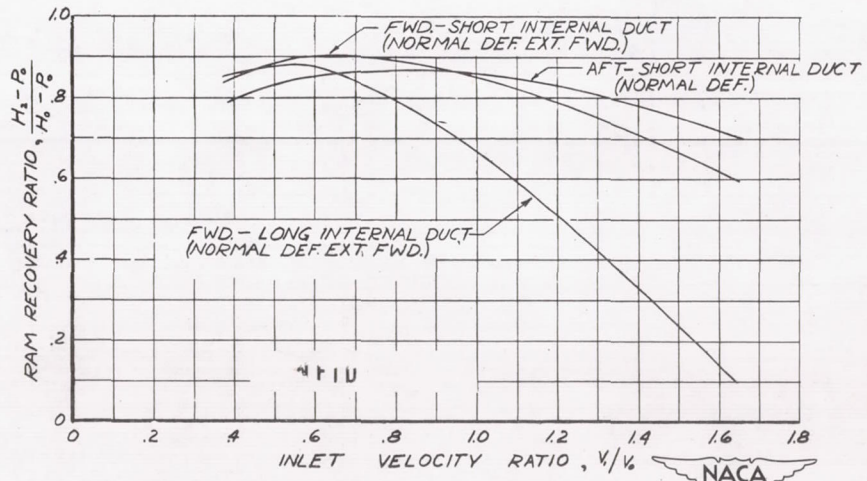
FIGURE 16. - VARIATION OF THE RAM RECOVERY RATIO AT THE SIMULATED COMPRESSOR ENTRANCE WITH ANGLE OF ATTACK FOR THE AFT SUBMERGED INLETS. SHORT INTERNAL DUCTING.



(a) PARALLEL WALLS

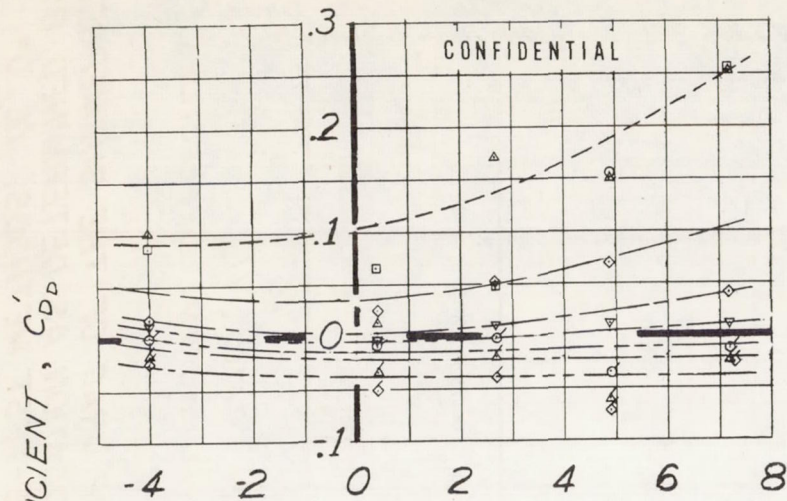


(b) DIVERGENT WALLS

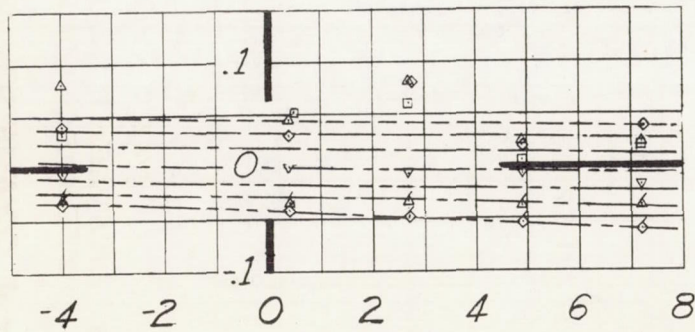
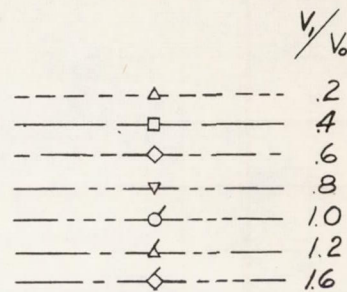


(c) DIVERGENT WALLS WITH DEFLECTORS

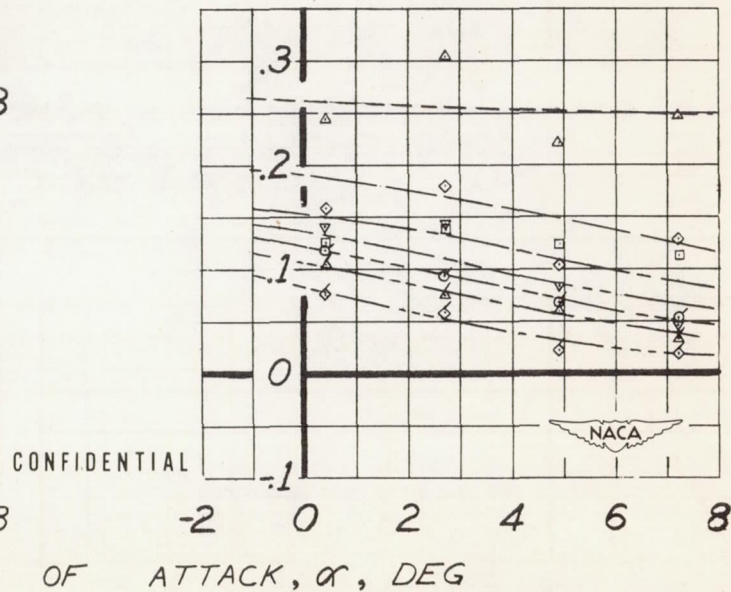
FIGURE 17. - RAM RECOVERY RATIO AT THE SIMULATED COMPRESSOR ENTRANCE WITH THE DIFFERENT INTERNAL DUCTS.  $\alpha, 0^\circ$ .



(a) PARALLEL WALLS



(b) DIVERGENT WALLS



(c) DIVERGENT WALLS WITH NORMAL DEFLECTORS EXTENDED FORWARD

FIGURE 18. - THE DRAG OF THE SUBMERGED AIR INLETS IN THE FORWARD LOCATION AS DETERMINED BY THE MOMENTUM METHOD.

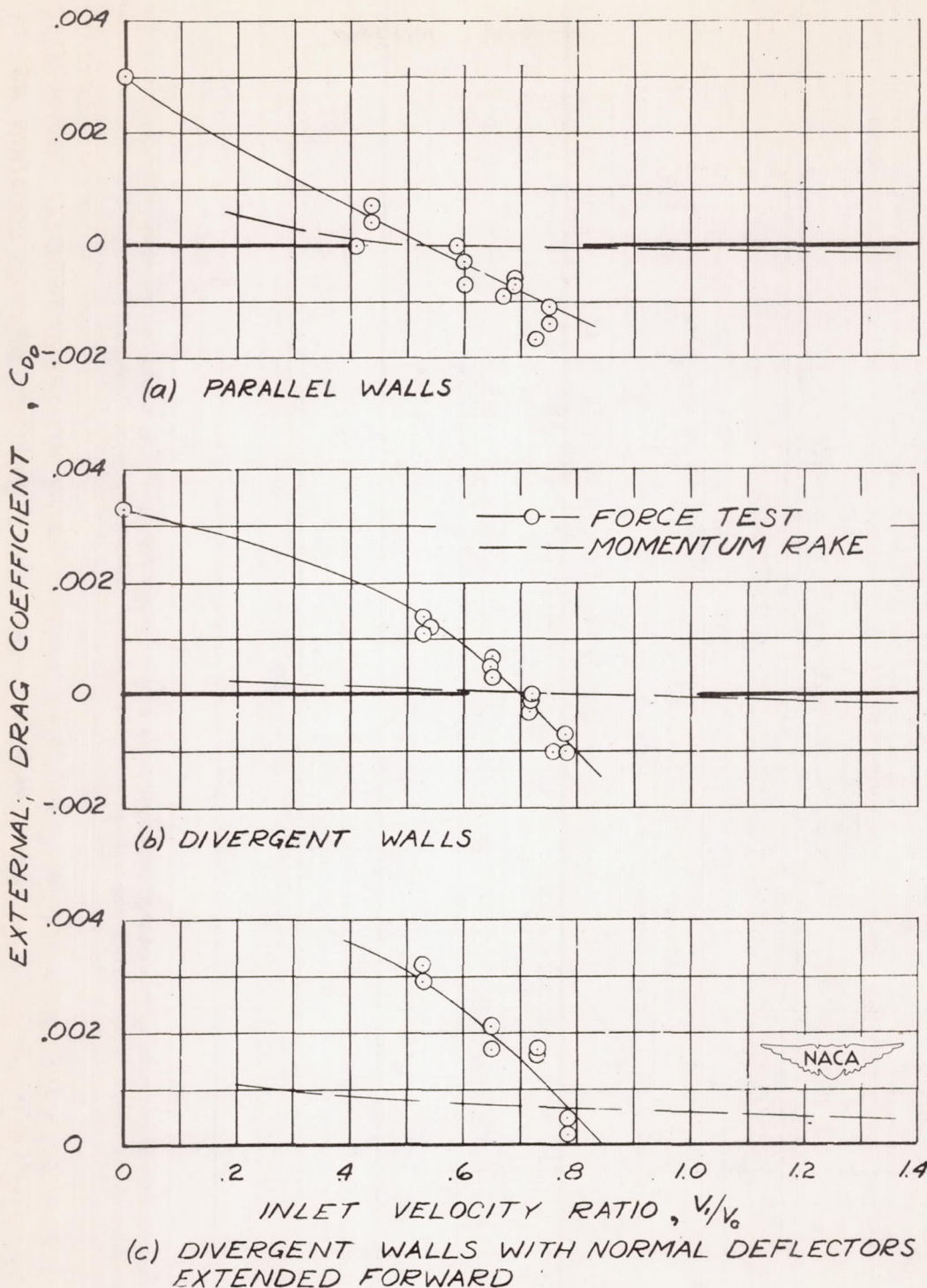


FIGURE 19. - A COMPARISON OF THE DRAG OF THE SUBMERGED AIR INLETS IN THE FORWARD LOCATION AS DETERMINED BY THE MOMENTUM AND THE FORCE-TEST METHODS.  $\alpha, 0^\circ$

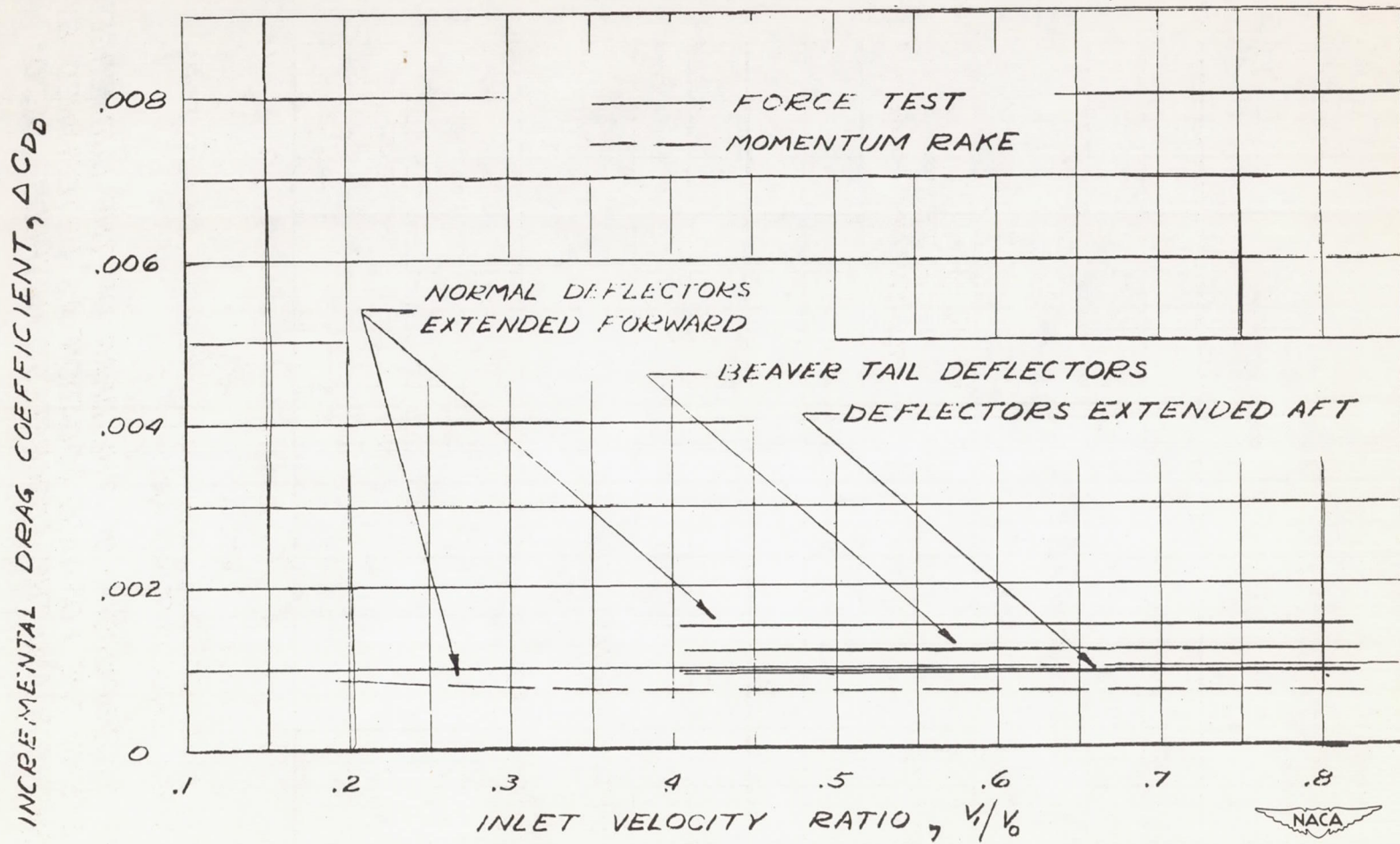


FIGURE 20.- THE VARIATION WITH INLET-VELOCITY RATIO OF THE DRAG INCREMENT DUE TO SEVERAL DEFLECTORS. FORWARD LOCATION OF THE INLET ;  $\alpha$ ,  $0^\circ$ .



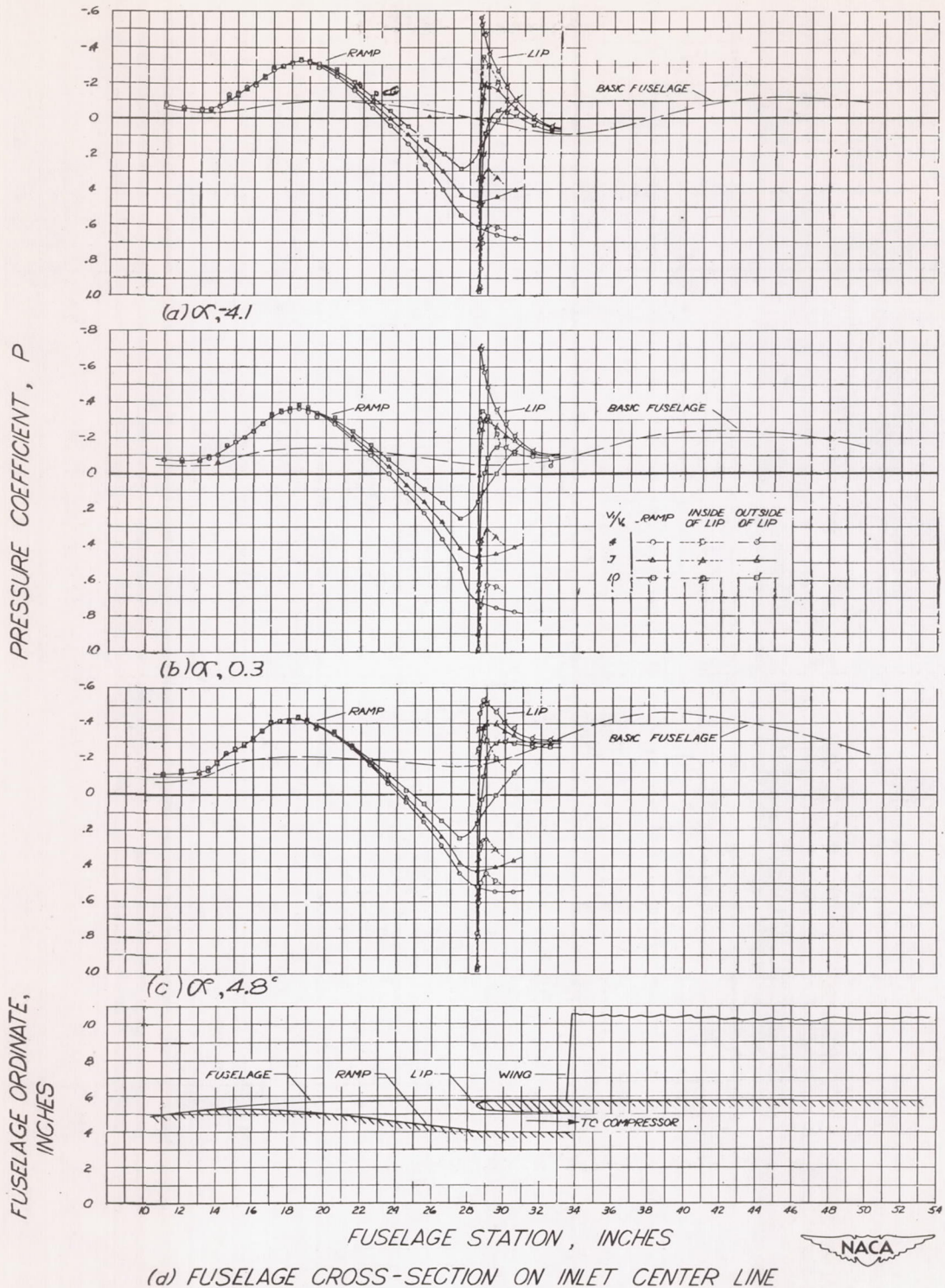


FIGURE 21. - PRESSURE DISTRIBUTION MEASURED ON THE CENTER LINE OF THE FORWARD INLET WITH THE DIVERGENT-WALLED RAMPS.



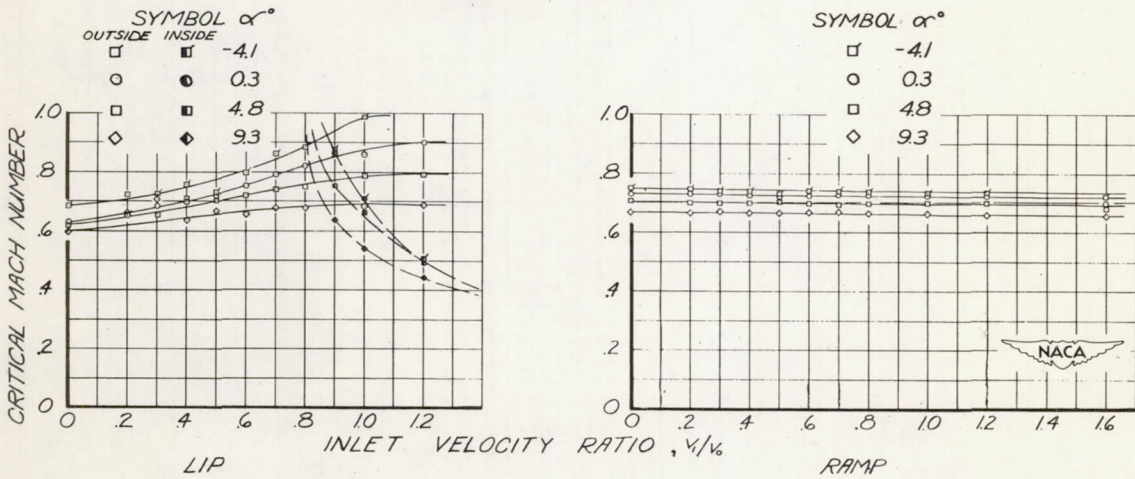
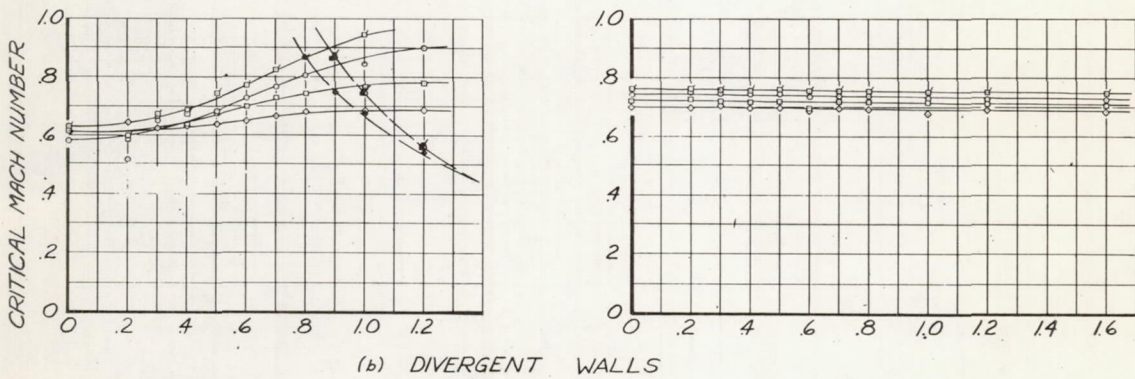
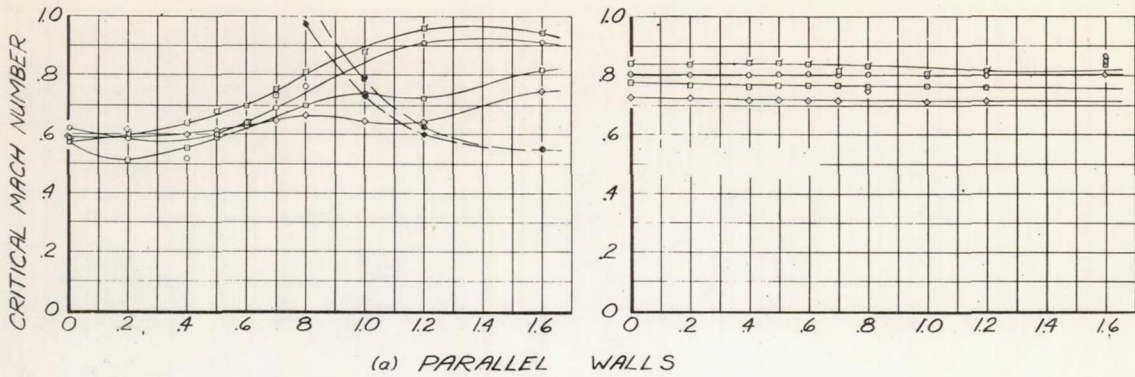


FIGURE 22. - VARIATION OF THE PREDICTED CRITICAL MACH NUMBER WITH INLET-VELOCITY RATIO FOR THE FORWARD LOCATION OF THE SUBMERGED INLETS.

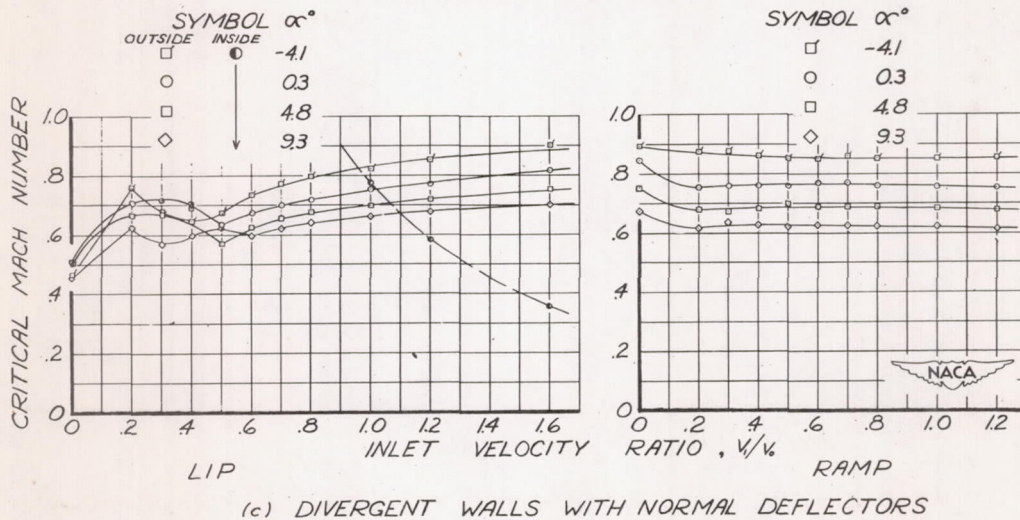
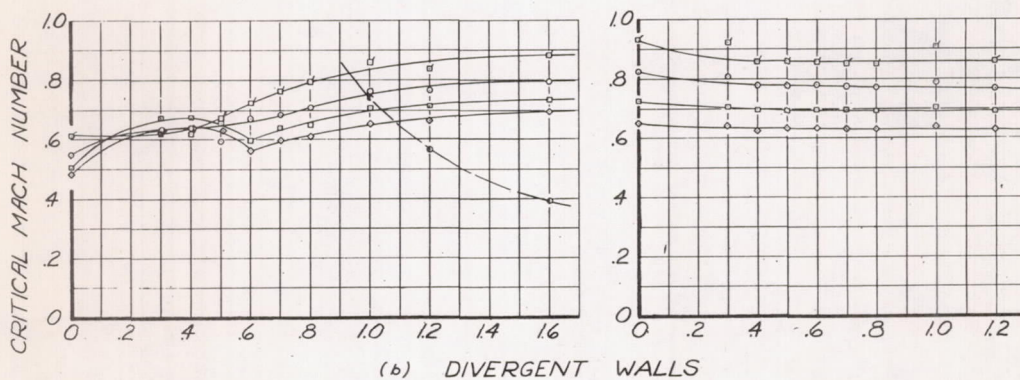
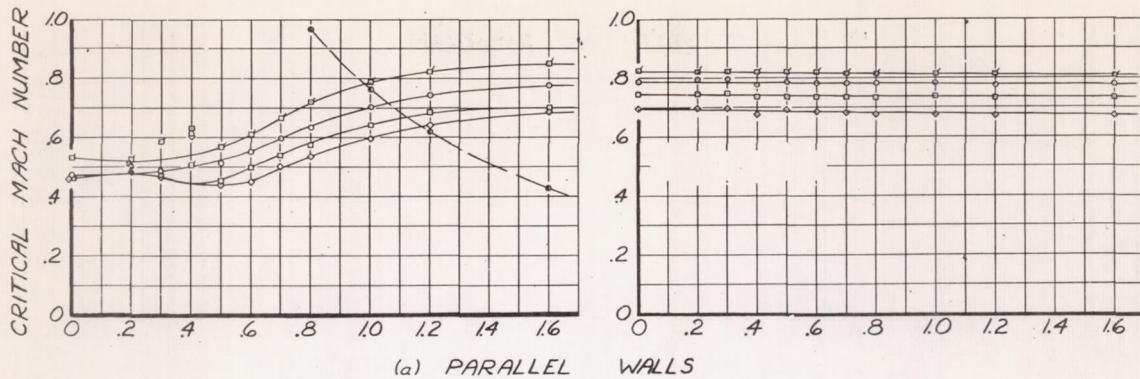


FIGURE 23. - VARIATION OF THE PREDICTED CRITICAL MACH NUMBER WITH INLET-VELOCITY RATIO FOR THE AFT LOCATION OF THE SUBMERGED INLETS.

